2007

Tornado-induced wind loads on a low-rise building

Vasanth Kumar Balaramudu
Iowa State University

Recommended Citation

Balaramudu, Vasanth Kumar, "Tornado-induced wind loads on a low-rise building" (2007). *Retrospective Theses and Dissertations*. 14860.
https://lib.dr.iastate.edu/rtd/14860

Tornado-induced wind loads on a low-rise building

by

Vasanth Kumar Balaramudu

A thesis submitted to the graduate faculty

in partial fulfillment of the requirements for the degree of

MASTER OF SCIENCE

Major: Aerospace Engineering

Program of Study Committee:
Fred Haan, Major Professor
Partha Sarkar
Vinay Dayal

Iowa State University

Ames, Iowa

2007

ProQuest Information and Learning Company
300 North Zeeb Road
P.O. Box 1346
Ann Arbor, MI 48106-1346

TABLE OF CONTENTS

LIST OF FIGURES

LIST OF TABLES

ABSTRACT

The effects of wind loading on buildings due to straight line boundary layer type winds have been studied extensively in the past. Building code estimates are mainly based on these works. Little research has been, however, done to study the effect of tornado winds on built structures. This research work essentially deals with the study of the effects of tornado type wind loading on low-rise buildings. Extensive testing was performed on a scaled down low-rise gable roof building model (1:100) to understand the loading pattern. The vortex generated using the ISU tornado simulator agreed well with the Doppler radar data from the Spencer, South Dakota tornado of May 30, 1998 and the Mulhall, Oklahoma tornado of May 3, 1999. The building model was tested using tornado vortices with five different core radii. The tornado could be translated using a crane mechanism; this enables realistic recreation of the actual effects on the low-rise building due to a moving vortex (which is the case in real world). The building model was also tested for four different vortex translation speeds. The lowest speed cases invariably produced larger loads. The effect of building orientation was also investigated by testing the model at seven different angles of attack. The results showed higher wind loads for the smallest vortex core with lower translation speeds. The building orientation of 60 deg had a higher loading pattern. In general the force and moment coefficients were higher than current building code provisions. Further wind tunnel tests were also carried out to study the effects of different roof types and building heights

CHAPTER 1. GENERAL INTRODUCTION

Introduction

Tornadoes are large scale intense vortex, which occurs during the thunderstorms. The tornado is formed when the rotating mass of air at the centre of the cloud extends downward. The tapering on the vortex funnel near the ground results in tremendous winds, due to vorticity and conservation of angular momentum. Every year, these high speed winds cause immense destruction to the life and property. Nearly 1000 tornados are reported every year in US. Annual damages can exceed over one billion dollars. The intensity of the tornado is rated using Fujita scale, which is based on the damages caused by the tornado. The Fujita scale is divided in to 5 levels, the lowest being F0 (40-72 mph) and highest is F5 (261-318 mph). But 90% of the tornados are rated F2 (113-157 mph) or less. Currently, the low-rise buildings are designed for lower wind speeds based on the building codes. For example, in the region called *Tornado Alley* the buildings are designed for a wind speed of 90 mph. There is little research done to estimate the wind loads on built structures due to tornados. The building code can be improved to cater for the effect of tornados; this will result in fewer losses in life and property damage. Hence the objective of this research work is to estimate the force and moment coefficients due to the tornado type winds of F2 intensity and compare it with the building code estimates. Large amount of wind tunnel tests were carried out to understand the effect of different vortex structures, the orientation of the building and the translation speed of the tornado. Similar tests were performed to study the influence of the roof shapes and the height of the building model. The following section outlines the thesis format.

Thesis Organization

This thesis is organized for the paper format. The Chapter 1 gives the general introduction about the effects of tornado on the built structures and the thesis organization of the thesis. Chapter 2 is based on the journal paper submitted to *Journal of Structural Engineering.*

This Chapter deals with the major findings and important results for the one story gable roof building model with a roof angle of about 35^0. The organization of the paper in Chapter 2 is as follows. Section 1 gives the introduction and relevant background study for the present research and defines the research objective. This section contains extensive literature review on the damages caused by tornado in terms of life and property damage. The experimental approach is given in section 2. It gives the physical dimension and related technical details of the ISU tornado simulator. The Tornado flow fields that are generated in this simulator are explained. The in-depth flow field analysis is given in Appendix-A. Section 2 also deals with the description of pressure and force model used for the tests and the related instrumentation and the test matrix. The normalization and the tornado loading characteristics are explained in Section 3. The localized peak pressure distribution for different vortex locations over the building model are also explained in the same section. The analysis and the discussions of the Force and Moment coefficients are given in section 4. The coefficient of force and moment comparison with the building code estimates are described in Section 5. This section also gives information about the scaling factors used to convert the model scale data to full scale estimates and it is followed by the conclusion and the relevant references. The next section contains the tables and the corresponding figures. Chapter 3 gives additional details on the analysis carried out on different building models. This section contains a brief introduction, details of the building models tested and the related results and discussion. The relevant table and the figures are listed in the same sequence. The conclusion for the present work and few recommendations for future work are explained in Chapter 4. This is followed by Appendix-A which gives more detailed information about the structure of the vortex and related work carried out previously by this group. Acknowledgements are given after chapter 4. The additional material regarding the structure of the vortex is given in Appendix A, Chapter 5. This section is an excerpt from "*"Design, Construction and Performance of a Large Tornado Simulator for Wind Engineering Applications - Engineering Structures in press, Dr Haan et al, 2007"*. The radial and azimuthal velocity profiles are discussed here.

CHAPTER 2.

TORNADO-INDUCED WIND LOADS ON A LOW-RISE BUILDING

A paper has been submitted to the Journal of Structural Engineering

Fred L. Haan, Jr.[*]
Assistant Professor
Department of Aerospace Engineering
2271 Howe Hall, Room 2341
Iowa State University
Ames, IA 50011-2271
USA
Ph : (515) 294-2884
E-mail: haan@iastate.edu

Vasanth Kumar Balaramudu
Graduate Research Assistant
Department of Aerospace Engineering
2271 Howe Hall, Room 1365
Iowa State University
Ames, IA 50011-2271
USA
E-mail: vasanth@iastate.edu

Partha P. Sarkar
Professor and Wilson Chair
Department of Aerospace Engineering
2271 Howe Hall, Room 2343
Iowa State University
Ames, IA 50011-2271
USA
Ph : (515) 294-0719
E-mail: ppsarkar@iastate.edu

---

[*] Corresponding author

Abstract

Current design wind loads for buildings and other structures are based upon model tests in low-speed boundary-layer wind tunnels that generate straight-line winds. Winds resulting from tornadoes that could occur during storm events such as thunderstorms or hurricanes differ greatly from conventionally-conceived atmospheric boundary-layer winds. This paper presents transient wind loads on a one-story gable-roofed building in a laboratory-simulated tornado and compares them with building code estimates. Tornadoes were simulated in smooth open terrain with vortex core diameters from 0.46 m to 1.06 m. A 1:100 scale model of a building with dimensions of 9.1m x 9.1m x 6.6 m and gable roof angle of 35° was used for this study. Comparisons of peak loads measured in this study showed that tornadoes of F2 strength would generate loads significantly greater than those prescribed by ASCE 7-05 for 40 m/s (90 mph), 3-sec gust, straight-line wind over open terrain.

2.1 Introduction

Low-speed boundary-layer wind tunnels generating straight-line winds have been used for a long time to develop design wind loads for buildings and other structures. Velocity fields resulting from some extreme wind events such as thunderstorms, microbursts and tornadoes, however, differ significantly from conventional atmospheric boundary-layer type events. Tornadoes are vortices with significant tangential and vertical velocity components. In the U.S., 1000 tornadoes occur annually and cause 60 deaths on average (Grazulis 1993). Tornadoes have occurred in all fifty states in the US with more frequent occurrence in what is known as “Tornado Alley” and they can occur in coastal regions as hurricanes make landfall.

In the past, large-scale damage and heavy loss of life were caused by intense tornado outbreaks in populated areas (Grazulis 1993; Brooks and Doswell 2001; Speheger et al 2002; Doswell et al. 2006; Forbes 2006). The Tri-State Tornado of 18 March 1925 killed 695 people and the Natchez, MS tornado of 7 May 1840 claimed 317 lives. The 1965 Palm Sunday Outbreak was the second deadliest of the 20th century, killing 258 people and injuring 3,148. The Oklahoma City tornado (May, 1999) stands as the costliest tornado in US history having destroyed nearly 11,000 buildings. The damage from the May 1999 outbreak as a whole amounted to about $1.5 billion. In 2003, between May 1 and May 11, 395 tornadoes touched down in the United States (Allaby 2004).

Tornadoes cause significant amounts of damage to buildings and most built structures are not designed to withstand these wind loads. Statistically 90% of all tornadoes are rated F2 or less (Bluestein and Golden 1993) on the Fujita Scale with maximum wind speeds less than 160 mph (3-sec gust). Hence it might be practical to design buildings to withstand these wind loads without escalating the building cost too significantly. The improvements in the building design must be made based on extensive wind tunnel testing. Numerical simulations are not feasible in terms of the computational resources required to capture the complex flow-structure interaction. Specialized wind tunnels are required to simulate the tornado flow fields over building models.

Many laboratory simulator designs have been based on the pioneering work of Ward (1972). Subsequent efforts—based on the Ward model—at Purdue University (Church et al. 1979), the University of Oklahoma (Jischke and Light 1983) and by Davies-Jones (1976) employed various means to improve the similarity between laboratory simulations and full-scale tornado events. These laboratory simulations were aimed at greater understanding of the tornado vortex itself. To examine tornado-structure interactions Chang (1971), Jischke and Light (1983), Bienkiewicz and Dudhia (1993) and, more recently, Fouts et al. (2002) and Mishra et al. (2005) modified the basic laboratory tornado simulator design of Ward (1972) and added small building models with pressure taps. In some cases, these efforts found mean surface pressures to be significantly higher (3-5 times) in swirling, tornado-like vortices than in straight-line boundary layer flows for the same fluid velocity. Most of these studies were done using stationary vortices and did not include overall force predictions. In Sarkar et al. (2006) and Sengupta et al. (2006) a cubic building and a tall building model were tested using a translational vortex of two different radii. These studies showed that vortex translation does influence aerodynamics loading and that vortex translation speed may be inversely proportional to peak loading magnitudes.

The objective of the current work was to conduct a broad, systematic study of the aerodynamic loads generated on a typical one-story gable roof building model exposed to different sizes of tornadoes and to compare the loads to standard building code estimates (specifically, ASCE 7-05). The tornado simulator at Iowa State University (ISU) was used to generate these vortices (see Haan et al. 2007 for specific details of the facility). The experimental setup and the results of these tests are presented in the following sections.

2.2 Experimental Approach

2.2.1 Tornado Simulator

2.2.1.1 Details of the tornado simulator

Figure 1 illustrates the simulator concept with a schematic diagram, and Figure 2 shows a picture of the entire system suspended from its crane. A circular duct 5.49m (18 ft.) in diameter and 3.35m (11 ft.) high is suspended from a 4500 kg (5 ton) overhead crane so that it can translate along a 10.36m (34 ft.) long ground plane. A 1.83m diameter fan (maximum flow rate of the fan is 40.0 m3/s, 85,000 cfm) is mounted in the center of this duct to act as an updraft. A rotating downdraft is generated by redirecting the air from the updraft fan down in a 0.30m (1.0 ft.) wide annular duct. Rotation is imparted to the air in the duct with vanes at the top of the simulator. As the rotating air flows toward the center of the simulator, the fan updraft stretches the low-level vorticity into a tornado-like vortex. More details on the design and validation of this system can be found in Haan et al. (2007). The clearance between the translating duct and the ground plane allows a wide range of building models to be placed on the ground plane for testing. The maximum translation speed of the crane is 0.61 m/s (2 ft/sec). Accounting for the acceleration and deceleration distance at the beginning and end of the crane motion, the prototype simulator can translate for a distance of 3.35 m (11 ft) at a constant speed of 0.61 m/s (1.4 mph) or less.

2.2.1.2 Details of the vortex flow fields

To generate a wide range of tornado scenarios for this study, the tornado simulator flow fields were quantified for a range of inflow swirl magnitudes. The inflow swirl is controlled by vanes in the downdraft duct, and these vanes were set at five different settings to produce five different sizes of tornados (referred to as cases Vane1 through Vane5). The swirl ratio, an important parameter governing such vortical flows, was quantified for each case. The swirl ratio, S, is the ratio of the vortex circulation to the accompanying rate of inflow into the vortex. In this paper, swirl ratio was calculated according to the following expression: $S = \pi V_{\theta \max} r_c^2 / Q$ where $V_{\theta \max}$ is the maximum tangential velocity at the radius of maximum wind speed, r_c is the radius of the core (i.e. radius of maximum wind speed) and Q is the flow rate through the fan (the inflow rate).

A multi-hole pressure probe was used to quantify the velocity fields for each case. Specifically, a spherical 18-hole pressure probe (PS18 Omniprobe from Dantec) was used. This 18-hole probe is organized in a network of five-hole configurations that can measure flow angularity up to 165 degrees with respect to the probe axis. The probe calibration uses a local least square fit with this network of 5-hole configurations to provide accuracy of 2% for velocity magnitude and 1.5 degrees for velocity angle. The probe pressures were measured with a Scanivalve ZOC33/64Px electronic pressure scanner.

The ground plane was fixed at 45.7 cm (18 in.) below the exit of the downdraft duct and the fan speed was fixed at 33% of full speed. Data were sampled at the rate of 78 Hz for 26 seconds (due to data rate and storage limitations). Measurements were made for all the vane angle settings described above. Maximum tangential velocities varied from of 6.9 m/s to 9.7 m/s. The various tornado parameters like vortex radii, swirl ratios and flow rates and model Reynolds numbers are listed in Table 1.

Figure 3 shows tangential velocity profiles for all cases. These profiles that are normalized with the maximum tangential speed and the radius of maximum tangential speed of the case Vane3, illustrate the simulator's control of the size of the vortex. The vortex size varies by a factor of 2.3 from the smallest to the largest. These sizes correspond to vortex diameters of 0.23m to 0.53m (corresponds to 2.5 to 5.8 times the plan dimension of the building model). Normalized tangential velocity profiles for the Vane5 case at various elevations are shown in Figure 4 along with radar data from field tornadoes. The data, obtained from Wurman (2004, 2005), were acquired using Doppler on Wheels observations from the Spencer, South Dakota tornado of May 30, 1998 (Wurman and Alexander, 2005) and the Mulhall, Oklahoma tornado of May 3, 1999 (Wurman, 2005). Scaling the vortices with the core radius, r_c, and with the maximum tangential velocity, $V_{\theta_{\max}}$, collapses the data very well and shows good comparison with the field velocity profiles. More details of the validation of the simulator velocity profiles with radar data from the field can be found in Haan et al. (2007).

2.2.2 Pressure and Force Model Details

Vortex-induced pressures were measured on a model one-story gable roof building (nominally 1:100 scale) with a 91mm by 91mm (3.6 in. by 3.6 in.) plan and an eave height of 36mm (1.4 in). The gable roof angle of the pressure model is 35° and its maximum height is 66 mm (2.6 in). The model was constructed with plexiglass surface and contains pressure taps to measure the overall external pressure distribution. . Figures 5 and 6 show the building pressure model with the pressure tap distribution The roof contains a total of 54 pressure taps. The leeward side of the roof (when the building is fixed at zero orientation with respect to the translational direction of the vortex, Figure 6) contains 24 pressure taps. The windward side contains 19 pressure taps and the two triangular gable end sections contain 5 taps each and the building walls contain 9 pressure taps on each side. The surface pressures were measured using a high speed electronic pressure scanner.

To verify the pressure measurements, a geometrically identical model was constructed for testing with a force balance. The force model was constructed as a single unit using the rapid prototyping technique with an aluminum rod through the center as the main structural support. This rod was connected through a hole in the ground plane to the JR3 force balance.

2.2.3 Pressure and Force Instrumentation

Two high speed electronic pressure scanners (Scanivalve ZOC33/64Px) were used to measure the pressure distribution on the building model. Each scanner incorporates 64 individual piezoresistive pressure sensors. The pressure taps on the model were connected to these sensors using 15 inch long vinyl tubing. The static pressure for all pressure measurements was the laboratory ambient pressure outside the tornado simulator. The pressure model itself is shown in Figure 5 while the tap locations are illustrated in Figure 6. The pressure transducer was zero calibrated before the start of the measurement using standard calibration technique recommended by the manufacturer. The pressure signals were corrected off-line for the dynamic effects of the tubing. Data were sampled at the rate of 430 Hz (controlled by an external clock). The initiation of data acquisition and the crane movement were synchronized using a common external trigger.

The global wind loads on the force model were measured using an external force balance. The force balance was a JR3 load cell (Model 30E12A-I40) capable of measuring all three force and all three moment components. Data were sampled at the rate of 500 Hz. The initiation of data acquisition and the crane movement were synchronized using a common external trigger. The force model was tested mainly to validate the results from pressure measurements.

2.2.4 Test Matrix

Extensive tests were done on the pressure model to study the effects of different building orientations and the effects of various tornado sizes and translation velocities. The pressure model was tested with five different vortex sizes and in orientations with respect to the tornado translation axis from 0 to 90 degrees with a step size of 15 degrees. Figure 7 shows the building orientation with respect to the tornado translation axis. In each case tested, the tornado translation axis passed through the center of the building model. For all building orientations, four different cases of tornado translation speed were considered. The tornado was translated at 0.15 m/sec, 0.30 m/sec, 0.46 m/sec and 0.61 m/sec (the fastest speed possible with the current system). The test matrix for the pressure measurements is listed in Table 2. Each test conditions involved 10 repeat runs to study the statistical variance. In total, 140 different combinations of conditions were tested for this building model.

Because the purpose of conducting load cell tests was to validate the force and moment coefficients from the intergrated pressure measurements, only a small portion of the overall test matrix was repeated for load cell testing. The force model was tested in the smallest vortex (Vane1). The model was tested for 0° and 45° orientations with respect to the tornado translation axis. For both orientations, three different cases of tornado translation speed (0.15 m/sec, 0.30 m/sec and 0.61 m/sec) were considered. Table 2 lists which types of load cell tests were conducted in the overall test matrix. As in the case of the pressure measurements, each force test case involved 10 repeat runs.

2.3 Character of Tornado-Induced loading

While the details of the results of the entire test matrix will be described in the next section, this section summarizes the general character of the tornado-induced aerodynamic loading. This type of summary will aid the interpretation of the data in the subsequent sections.

Conventions Used to Present the Data

Many of the figures in this paper reflect the time-varying character of the tornado-induced loads. Rather than plotting these load histories with respect to time, these are plotted with respect to the distance betwen the center of the tornado vortex and the center of the building model (x) normalized by the diameter of the tornado core (D). In all cases, the tornado translates along the x-axis in the positive x direction starting from x/D values less than -10 (for axis reference, see Figure 7).

To compute x/D and to position the building model such that the tornado translation axis would coincide with its center, the center of the tornado vortex had to be located. This was accomplished by installing pressure taps on the ground plane and observing the surface pressure distribution as the tornadoes translated past. The building model was positioned in the path of the tornado center for each tornado case that was tested. The smaller-diameter tornadoes (such as the Vane1 case) had narrow surface pressure distributions with a well defined peak value that made the center of the vortex easy to locate. The larger-diameter cases, however, had much flatter surface pressure distributions (and greater fluctuations) that made the center more difficult to locate.

The overall forces and moments acting on the model were estimated by integrating the surface pressures. All force and moment coefficients for the tornado cases were normalized using the respective maximum tangential velocity of tornado (as shown in Table 1) and the area (S) of the side or top face of the model as illustrated in Figure 8. The coefficients were calculated using the following equations where S is the projected areas in the y direction, S_z is the project area in the z direction, h is the peak building height, and b is the building planform length:

$$\begin{aligned} C_{F_x} &= \frac{F_x}{\frac{1}{2}\rho V_{\theta_{\max}}^2 S} & C_{M_x} &= \frac{M_x}{\frac{1}{2}\rho V_{\theta_{\max}}^2 Sh} \\ C_{F_y} &= \frac{F_y}{\frac{1}{2}\rho V_{\theta_{\max}}^2 S} & C_{M_y} &= \frac{M_y}{\frac{1}{2}\rho V_{\theta_{\max}}^2 Sh} \qquad (1) \\ C_{F_z} &= \frac{F_z}{\frac{1}{2}\rho V_{\theta_{\max}}^2 S_z} & C_{M_z} &= \frac{M_z}{\frac{1}{2}\rho V_{\theta_{\max}}^2 S_z b} \end{aligned}$$

Character of the Tornado Loading Data

Figure 9 shows time histories of C_p on the walls of the building model (Wall ports # 5, 14, 23 and 32) for Case 1 (0° building orientation with the smallest vortex size (Vane 1) and slowest vortex translation speed (0.15 m/s)). The flat portion of the signal (for large negative values of *x*/*D*) corresponds to the situation where the tornado simulator's downdraft duct has not yet reached the model. Each pressure signal then shows a similar large negative pressure as the core of the vortex passes. The maximum C_p magnitudes occur when the vortex center passes over the top of the model. Pressure signals such as these were then integrated to obtain force and moment coefficients.

To illustrate the character of each of the force signals, Figure 10 plots each of the force coefficients relative to each other. The C_{F_x} signal shows that the tornado draws the building toward itself—possibly due both to the large static pressure drop that the vortex generates and the radial winds moving toward the vortex center. As the tornado moves from the negative to the positive x direction, C_{F_x} shows the model pulled first in the negative direction and then in the positive direction. The C_{F_y} signal follows the pattern of the tangential velocity component of the vortex. The tangential velocity of the vortex exerts a positive C_{F_y} as the vortex core first encounters the model. As the opposite side of the core passes the model, the sign of C_{F_y} changes. The side force (C_{F_y}) is higher than the axial force (C_{F_x}), since the tangential winds are stronger than the radial winds. The peaks for C_{F_x} and C_{F_y} occur very close to $x/D \sim 0.5$ (is the radius of the vortex). The uplift force (C_{F_z}) has a larger magnitude than the other two force components. The character of C_{F_z} is primarily due to the suction caused by the vortex core. This can be seen from the fact that maximum C_{F_z} occurs at $x/D = 0$. The moment coefficients are plotted in Figure 11. Due to the large side force, C_{F_y}, the corresponding bending moment, C_{M_x}, has a significant effect on the structure. Figure 12 illustrates the typical variance among ensembles by showing the integrated C_{F_y} profile ensemble averaged over the 10 identical runs of Case1 and shows the signal's upper and lower bounds computed for 95% confidence interval (mean value plus and minus 2.262 times the sample standard deviation)

The force and moment coefficients integrated from pressure measurements were compared with the results from the load cell measurements to check consistency. The load cell tests and pressure tests were conducted on two different models (with identical dimensions) under equivalent laboratory conditions. The three forces and three moments acting on the model were directly obtained from the load cell, whereas in the pressure measurement they were obtained by integrating the surface pressures. Except for C_{F_z} , forces and moments obtained from the two methods were very similar as exemplified in the Case1 comparison of C_{F_y} in Figure 13. The C_{F_z} comparison in Figure 14, however, shows that the pressure measurements predict much larger uplift forces than do the force measurements. The different predictions from these two measurement techniques are most likely due to the influence of internal pressure on the force measurements. The primary evidence for this comes from the fact that only the C_{F_z} predictions show a difference between force and pressure measurements. Since in the other coefficient predictions, the internal pressure effect cancels out are not be affected. However in the pressure measurement technique where only external pressures are measured they would not be affected by the internal pressure acting on the roof as would the force measurements. Because real buildings are not perfectly sealed, future work must address the issue of internal pressure systematically.

The vortex translation speeds were observed to have a significant effect on the magnitude and the nature of the load profile. Figures 15 and 16 summarize the character of this effect by plotting ensemble average time series of C_{F_y} and C_{F_z} force components for Cases 1, 3 and 4, that is, for translation speeds of 0.15, 0.46 and 0.61 m/s respectively. The overall magnitude reduces with the increase in the translation speed. This implies that slower moving tornadoes may cause more damage than the faster moving ones.

With respect to tornado translation effects, another interesting observation can be made from these figures. The entire loading profile shows a shift relative to translation speed. The faster moving vortex exhibits a greater x-direction shift compared to the slower moving vortex. This can be at least partially explained with the illustration of Figure 17. While this phenomenon has not yet been directly measured, the illustration represents flow visualization observations that show the portion of the vortex near the ground lagging behind the portion of the vortex close to the fan. Hence a vortex in translation can strike the building with its lower portion after the upper part of the vortex has passed the model. Because the x/D distance used for plotting is referenced to the center of a *stationary* vortex (as quantified during velocity measurements), the loading profiles are not symmetric around $x/D = 0$.

Pressure Distributions Around the Building Model

As an example of a pressure distribution, Case 17 (60° building orientation with the smallest vortex size (Vane 1) and slowest vortex translation speed (0.15 m/s)) was plotted because it exhibited some of the largest peak loads. Figure 18 gives the distribution of the local peak pressure coefficients, $C_{\hat{p}}$. The $C_{\hat{p}}$ plot shows symmetric loading on the roof and the walls.

The peak pressure occurs at the corners of the roof. Figure 19 shows the instantaneous C_p distribution when the vortex had not yet reached the building and was at $x/D = -0.45$ (the location corresponding to one of the peaks in the C_{F_y} time history as exemplified in Figure 10). Maximum pressure loading occurs at the leeward side of the roof and wall. Figure 20 reports the instantaneous C_p values when the vortex was past the building at (the location that corresponds to the minimum C_{F_y} value as in Figure 10). In this case, maximum pressure loading occurred at the leeward side of the roof and wall.

2.4 Tornado Parameter Study

This section summarizes the results of the previously-described test matrix, that is, tests from five different vortex sizes, four vortex translation speeds and seven building orientations. are summarized in this section. For each case of the test matrix, the maximum and minimum peak values of the force and moment coefficients were acquired. Essentially this means finding the maximum and minimum values from the time history plots described in Section 3. The maximum and minimum values correspond to average of the peak values obtained from 10 identical runs (not the peak from the ensemble average). These coefficients were normalized according to the conventions of Eqns. (1) and are plotted as open symbols in Figures 21 to 26.

$C_{\hat{F}_x}$ in Figure 21 is the coefficient of peak force in the direction of the vortex translation. The largest $C_{\hat{F}_x}$ values were somewhat similar across different vortex sizes. In general, peak axial force magnitudes were higher for building orientations of 0°, 15° and 75°, 90° than for 30°, 45° and 60°. Vane1 through Vane3 cases, the smaller tornado diameters, showed a symmetric distribution for maximum and minimum peaks. This symmetry was not seen for the larger diameter vortices of the Vane4 and Vane5 cases. This is most likely due to the center of the model not being exactly aligned with the vortex translation axis as described in Section 3. The effect of vortex translation speed is also clearly evident. In most cases, slower translation speeds generated larger magnitude peaks.

$C_{\hat{F}_y}$ is the coefficient for the peak transverse forces (see Figure 22), the forces that are perpendicular to the vortex translation axis. The largest values in the $C_{\hat{F}_y}$ distribution occur at 45° and 60° building orientations with smaller values near 0° and 90°. Vortex translation speed appears to have the same effect on $C_{\hat{F}_y}$ as on $C_{\hat{F}_x}$. In addition, a somewhat larger peak magnitudes were observed for the smaller diameter vortices (with the Vane1 cases having peak forces as much as 40% larger than the Vane5 cases.).

The peak uplift force ($C_{\hat{F}_z}$) values of Figure 23 did not show a significant variation with respect to the building orientation. This may be due to the uplift force mainly being caused by the low static pressure zone created inside the vortex core rather than the aerodynamic interaction of the roof with the flow. As with the other forces, the loads were higher for the slower-moving and smaller-diameter tornadoes. The smaller diameter vortices generated peaks approximately 40% larger than those of the larger diameter vortices.

The $C_{\hat{M}_x}$ and $C_{\hat{M}_y}$ components had similar trends as shown in Figures 24 and 25. The peak loads occured at 45° to 70° orientations of the building model. The maximum and minimum distributions are fairly symmetric for most of the vane cases. The peak values for C_{M_y} occurred at 0° orientation of the model (Figure 26). The magnitude and the trends were very similar for different vortex sizes. The effect of twisting moment ($C_{\hat{M}_z}$) was uniform across the cases and did not show significant magnitude.

To quantify the precision uncertainty for the peak estimates, the C_{F_y} peak values were plotted in Figure 27 in terms of 95% confidence intervals computed as plus and minus 2.262 times the sample standard deviation of the mean peak values. The uncertainty in these peak values then ranged from about ±7% to ±10%.

2.5 Comparison with Building Code

In this section, the peak values described in the previous section were compared with ASCE 7-05 provisions. To make this comparison, the force and moment coefficients defined according to Eqns. (1) had to be converted to use a normalization consistent with that used by ASCE 7-05. This section first describes this conversion and then discusses the comparison of the measured coefficients with the main wind force resisting system provisions and with the components and cladding provisions of ASCE 7.

5.1 *Converting Force Coefficients*

ASCE 7-05 provisions involve a dynamic pressure corresponding to 90 mph, 3-second gust peak velocities. In order to compare the tornado simulator measurements with coefficients from the building code, the laboratory values needed to be rescaled according to some full scale equivalent. What was desired was a peak force coefficient that is normalized with a dynamic pressure corresponding to a 3-second gust velocity. This would allow a consistent comparison with the coefficients of ASCE 7-05. The approach described below essentially estimates a full-scale peak force value and normalizes it with a full-scale 3-second gust dynamic pressure.

One can begin this approach by considering the definition of the peak force coefficient, $C_{\hat{F}}$, which is the normalized form of the peak forces, $\hat{F}$, measured during the laboratory tests. The fundamental assumption required to extrapolate model scale peak force values to full scale is that the peak force coefficients at both scales are equivalent, that is:

$$C_{\hat{F}_m} = C_{\hat{F}_{fs}} \tag{2}$$

where the subscripts *m* and *fs* denote model and full scale, respectively. $C_{\hat{F}_m}$ and $C_{\hat{F}_{fs}}$ are simply the peak force values normalized by the dynamic pressure, *q*, and frontal area, *A*, as:

$$C_{\hat{F}_m} = \frac{\hat{F}_m}{q_m A_m} \qquad\qquad C_{\hat{F}_{fs}} = \frac{\hat{F}_{fs}}{q_{fs} A_{fs}} \tag{3}$$

The model scale dynamic pressure, q_m, is defined as $q_m = \frac{1}{2}\rho\left(V_{\theta_{\max}}\right)_m^2$ where $\left(V_{\theta_{\max}}\right)_m$ is the model-scale maximum tangential velocity measured with the model scale averaging time (denoted as τ_m). As mentioned previously, the model scale averaging time for these tests was 26 sec. For these coefficients to be consistent with each other, one must assume that the full-scale averaging time for q_{fs} is a full-scale equivalent of the model scale averaging time of q_m.

Wind speeds are typically converted from one averaging time to another using some form of equation (4) found in Simiu and Scanlan (1996) and using statistical data on wind speeds found in such references as Durst (1960).

$$V_\tau(z) = V_{3600}(z)\left(1 + \frac{\beta^{1/2} c(\tau)}{2.5 \ln(z/z_0)}\right) \tag{4}$$

where $V_\tau(z)$ is the wind speed at elevation z with averaging time τ, z_0 is the aerodynamic roughness length, β is constant of proportionality between the square of the friction velocity and the variance of the turbulent velocity fluctuations (specifically, $\sigma_u^2 = \beta u_*^2$ where u_* is the friction velocity and σ_u^2 is the variance the velocity fluctuations), and $c(\tau)$ is a coefficient dependent on averaging time and derived from statistical wind studies (in this case, from Durst, 1960).

Using such an approach to convert wind speeds for tornadoes is problematic for two primary reasons. First, equation (4) assumes a logarithmic velocity profile typical of straight-line boundary layer flow, and second, the only statistical data available for quantifying the coefficient $c(\tau)$ were derived from straight-line boundary layer flow. To date, the velocity profile and turbulent statistics within a tornado in the field have not ever been quantified.

Given this situation, the authors decided that the best approach for this project would be to assume (until more complete field data become available) that equation (4) is appropriate to adjust wind speeds for averaging times within a tornado. Equation (4) was then used assuming open terrain.

Because 90% of tornadoes are F2 or lower in intensity, it was decided to scale the laboratory data up to F2 wind speeds (upper limit), that is, to 70m/s (157 mph) for a 3-sec. gust. This 157mph had to be adjusted for an averaging time that was equivalent to the model scale averaging time of $\tau_m = 26\,\text{sec}$. The full scale averaging time to be used with equation (4) can be found from the model scale averaging time and the time scale to be $\tau_{fs} = \tau_m / \lambda_T$ where the time scale is given by by $\lambda_T = \lambda_L / \lambda_V$ (where λ_L and λ_V are the length and velocity scales, respectively). Since the time scale is a function of the velocity scale which in turn depends on the time scale according to equation (4), the time and velocity scales had to be found iteratively.

For the tornado cases shown in Table 1, the time scales were estimated from 1:13.8 to 1:19.6. The time scales vary because the maximum tangential velocities vary from one tornado case to the next. The full scale averaging time, τ_{fs}, then varied between 358.8 to 509.6 sec. At this averaging time, an F2 tornado speed (which is 70m/s for a 3-sec gust), renders a value of 65 to 67 m/s for $\left(V_{\theta_{\max}}\right)_{fs}$. The full scale dynamic pressure can then be estimated as $q_{fs} = \frac{1}{2}\rho\left(V_{\theta_{\max}}\right)_{fs}^{2}$. The full scale peak force value can then be written as shown in equation (5) below.

$$\hat{F}_{fs} \cong q_{fs} A_{fs} C_{\hat{F}_m} \tag{5}$$

This can now finally be written as a peak force coefficient, consistent with ASCE 7-05, by normalizing with a dynamic pressure given by a 3-second gust velocity of 70m/s as in equation (6).

$$C_{\hat{F}_{fs}} = \frac{\hat{F}_{fs}}{q_{70-3\sec} A_{fs}} = \frac{q_{fs} A_{fs} C_{\hat{F}_m}}{q_{70-3\sec} A_{fs}} = \frac{q_{fs} C_{\hat{F}_m}}{q_{70-3\sec}} \tag{6}$$

where $q_{70-3\sec}$ is the dynamic pressure obtained from a 3-second gust velocity of 70m/s.

The $C_{\hat{F}_{fs}}$ values resulting from equation (6) were plotted in Figures 21-26 as filled symbols. These full scale coefficient values show slightly lower magnitudes than the model-scale values. The next step was to compare these peak values with building code provisions.

2.5.1 *Main Wind Force Resisting Systems (MWFRS)*

ASCE 7-05 MWFRS load calculation for low-rise building (Eq 6.5.12.2.3) was used for estimating the building loads in open terrain (Exposure C) and homogenous topography. An importance factor of 1.0 (Category 2) was considered for the present analysis as was a design wind speed of 90 mph, 3-sec gust (the typical design wind speed of the "Tornado Alley" region of the central United States). Full scale building dimensions were used for the force and moment estimation. The coefficients were estimated for eight different building configurations and the worst case was compared with the full scale equivalent coefficients from the tornado simulator in Figures 21-25.

The $C_{\hat{F}_x}$ comparison (figure 21) shows the peak tornado coefficients vary from 0.14 to 1.43 times the building code provision. In general, the coefficients for 30°, 45° and 60° building orientation were comparable to or lower than the building code estimates. Figure 22 gives the $C_{\hat{F}_y}$ comparison. The tornado values varied from 0.55 to 2.09 times the building code. The overall tornado values were higher than the ASCE estimates except for 30° and 45° building orientations with the largest diameter tornado (Vane5). The peak uplift force coefficient, $C_{\hat{F}_z}$, varied from 2.5 to 3.72 times the building code and was plotted in Figure 23.

The peak moment coefficients $C_{\hat{M}_x}$ and $C_{\hat{M}_y}$ varied from 0.24 to 2.14 and 0.02 to 1.42, respectively, of the building code estimates. The significant lower values in C_{M_y} for the

Vane3, Vane4 and Vane5 cases on the negative side was probably due mainly to the path of the tornado not intersecting the center of the building model. This is clearly seen from Figure 25 where for larger diameter tornadoes, the maximum and minimum distribution was slightly shifted up and was not symmetric about the zero.

2.5.2 *Components and Cladding*

The design wind pressures on the components and cladding elements were calculated using Eq 6.5.12.4.1 from ASCE 7-05 for low-rise buildings with height lower than 60 ft. The loads were estimated for open terrain (Exposure C) and homogenous topography. For the present analysis, only the external pressures on the surface of the building are estimated and compared with the local worst case surface pressures measured from the laboratory experiment.

The scaling of the laboratory pressure coefficients were similar to that of the scaling carried out in the previous section. The model coefficients correspond to 26 sec averaging time of the wind speeds which is equal to full scale equivalent averaging time of 358.8 to 509.6 sec using corresponding time scale of 1: 13.8 to 19.6. The coefficients are then scaled for 3-sec full scale value using 157 mph for 3-sec gust.

Figure 28 gives the comparison between the coefficients of pressure (C_p) on the wall for the experiment and the building code. The roof C_p comparison between the two is shown in

Figure 29. The peak uplift force coefficient ($C_{\hat{F}_z}$) from ASCE-7-05 is a combination of positive and negative C_p on the roof, whereas the for the tornado simulator case it was negative throughout, hence the $C_{\hat{F}_z}$ variation between the tornado and building code show higher differences compared to the differences in C_p.

2.6 Conclusion

The goal of the work presented here was to subject a one story gable roof building model to simulated tornado winds to quantify the resulting aerodynamic loading on the building. Comparisons were made between ASCE 7-05 provisions and the tornado loads because building standard or code provisions are derived from straight-line wind tunnel data. The loads in tornadoes of F2 intensity were found to exceed the ASCE 7-05 design loads, as calculated for the small scale rigid building located in tornado alley of the continental United States. The peak values of side force coefficients exceed by a factor as high as 2.1 and the peak values of uplift force coefficients exceed by a factor of 3.7. Hence it is evident that the buildings constructed based of standard building codes will not withstand the wind loads created by tornadoes of F2 intensity.

Acknowledgements

The authors gratefully acknowledge the support of the National Science Foundation (CMS 0220006), the work of Bill Rickard and numerous undergraduate students from the ISU Aerospace Engineering Department who contributed to this project.

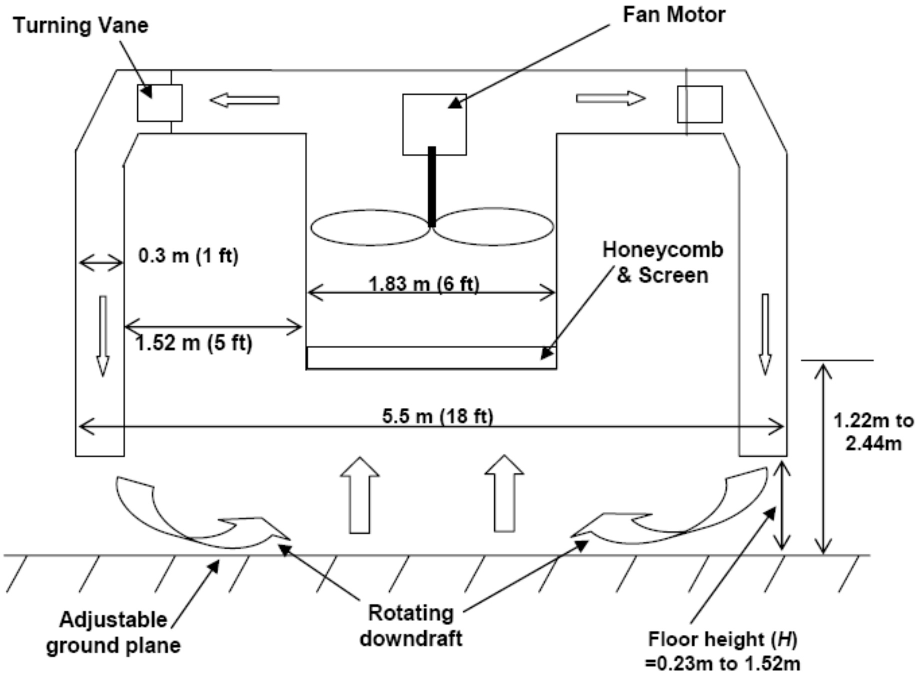

Figure 2-1: Schematic diagram of the ISU Tornado Simulator

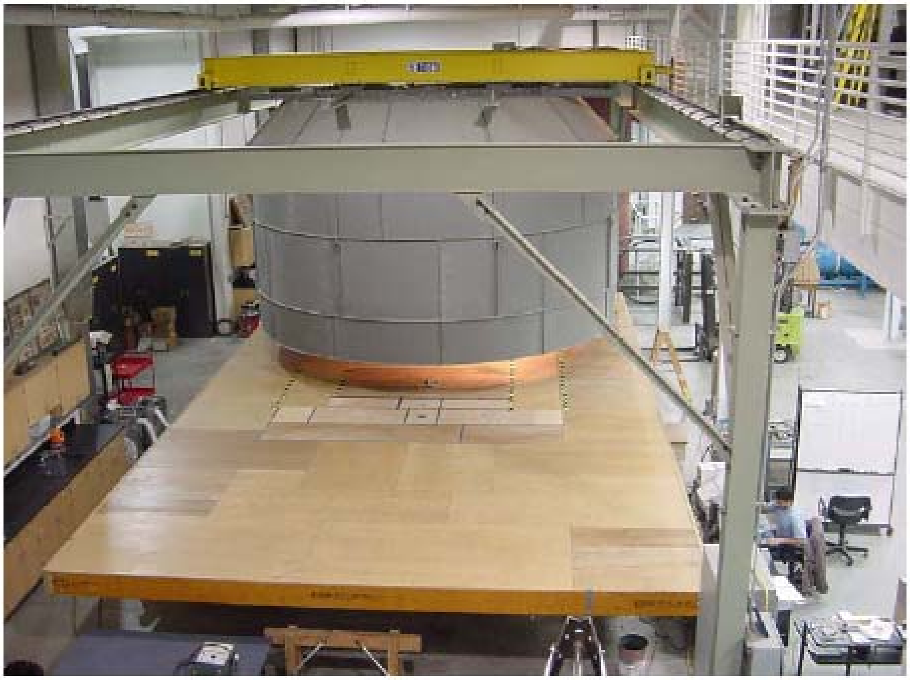

Figure 2-2: Photo of ISU Tornado Simulator

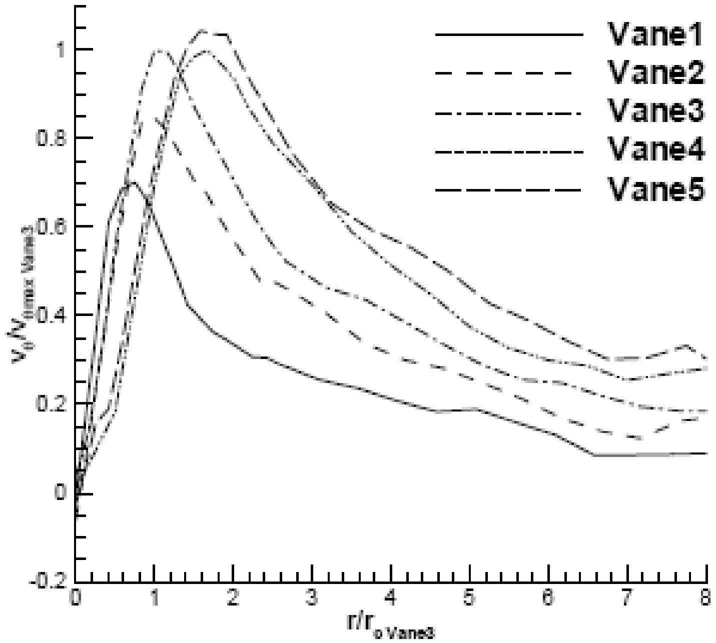

Figure 2-3: Tangential velocity profiles showing the change of vortex core radius with increasing vane angle.

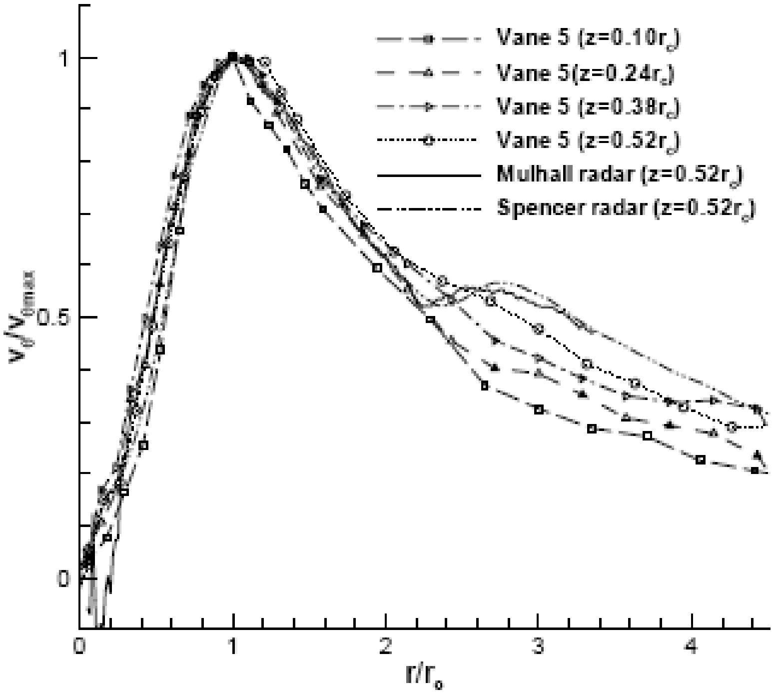

Figure 2-4: Scaled tangential velocity profiles for laboratory tornado case Vane 5 at different elevations along with full-scale Mulhall and Spencer tornado data (Wurman, 2004, 2005) at a specific elevation.

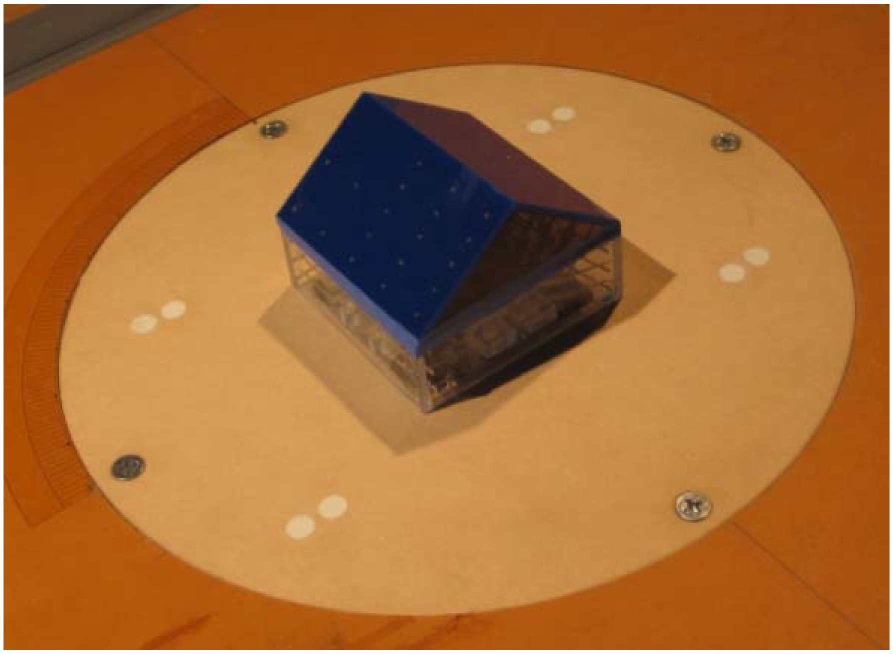

Figure 2-5: Photo of gable roof building model with pressure taps.

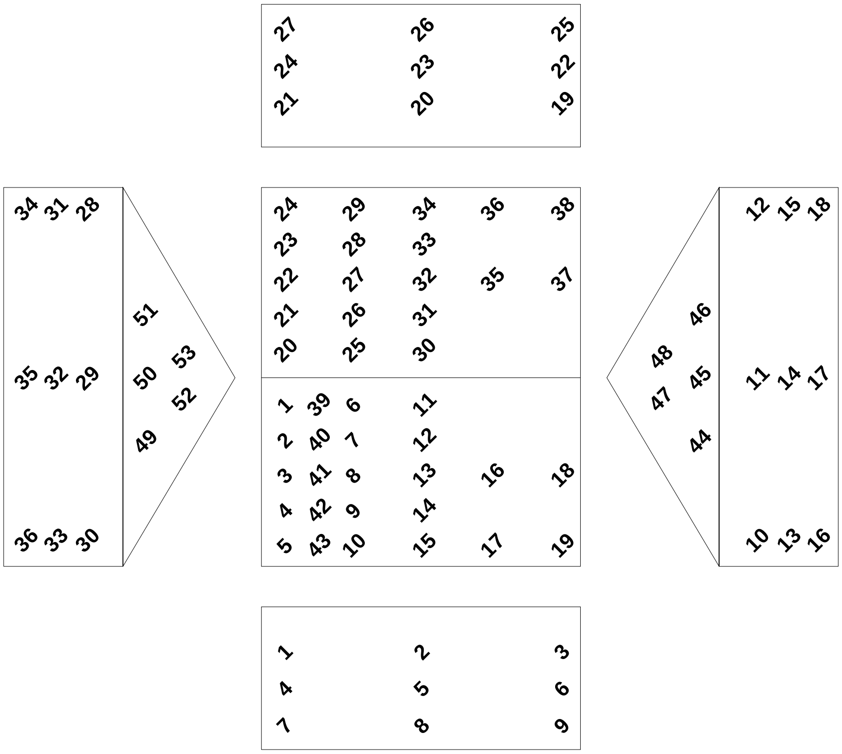

Figure 2-6: Exploded view of the gable roof building with pressure tap labels

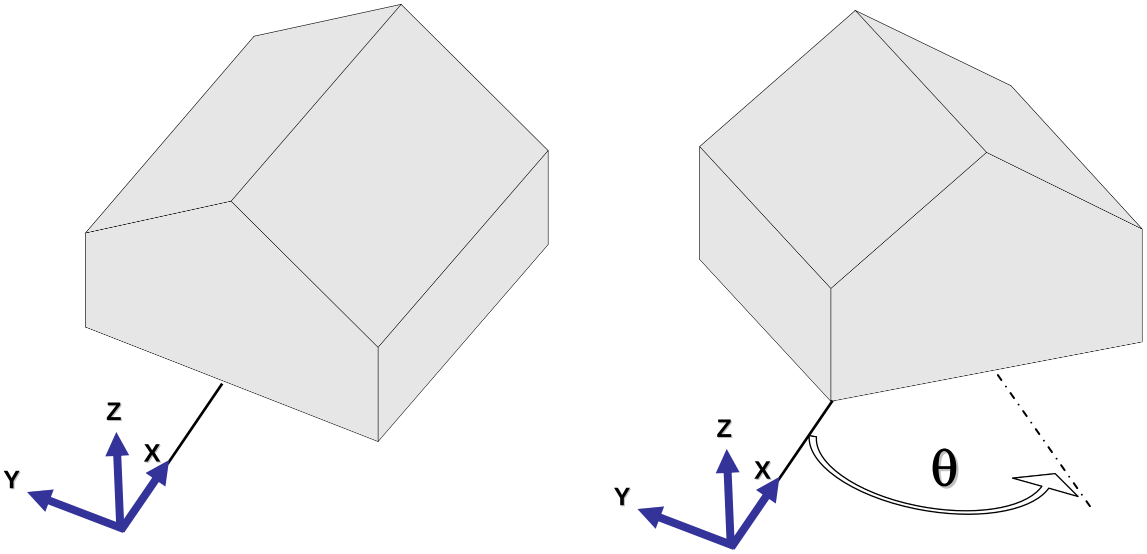

Figure 2-7: Building orientation with respect to the vortex translation direction (*x*-axis)

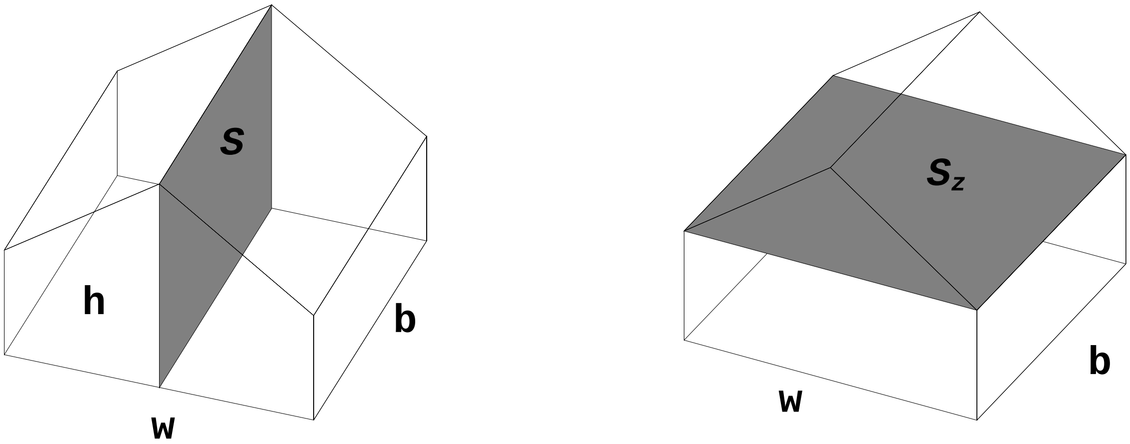

Figure 2-8: S is the projected area in the y direction,
S_z is the projected area in z direction

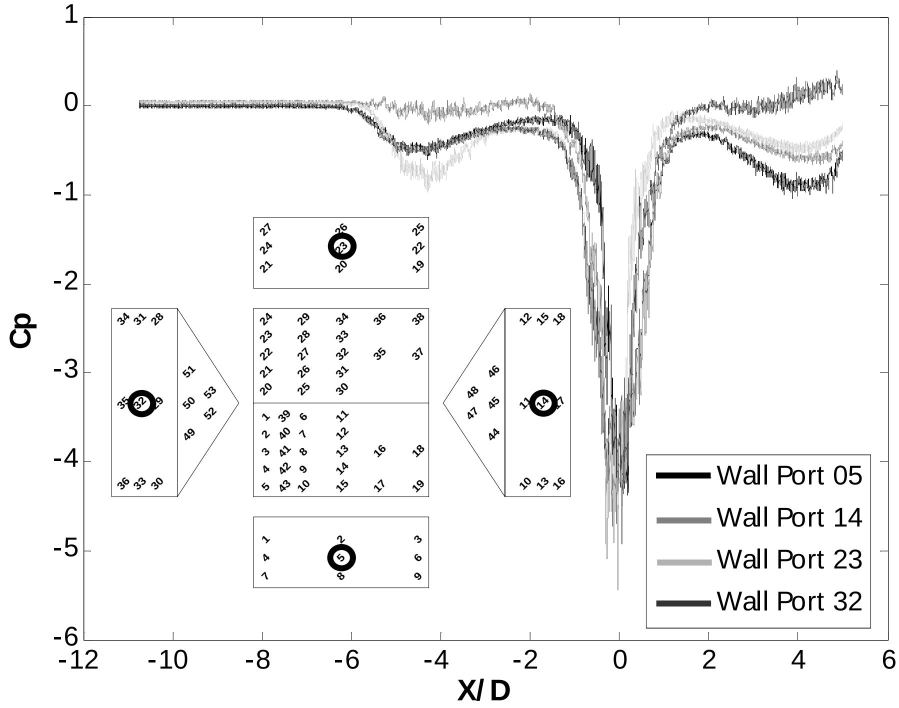

Figure 2-9: *Cp* time history at Wall Port # 5, 14, 23& 32 for Case 1

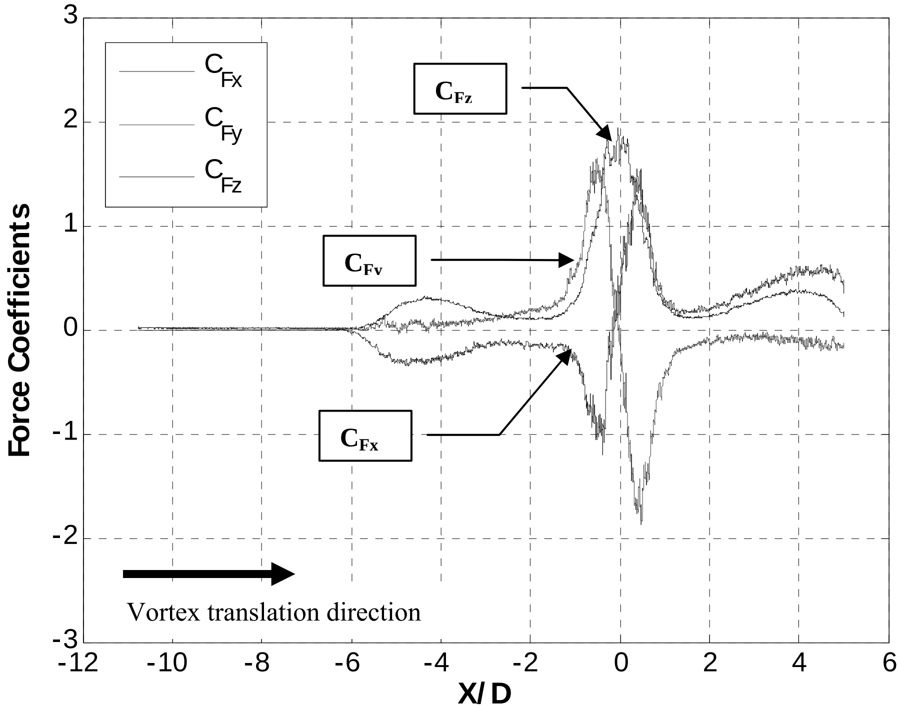

Figure 2-10: Time history of force coefficients showing relative magnitudes for Case 1

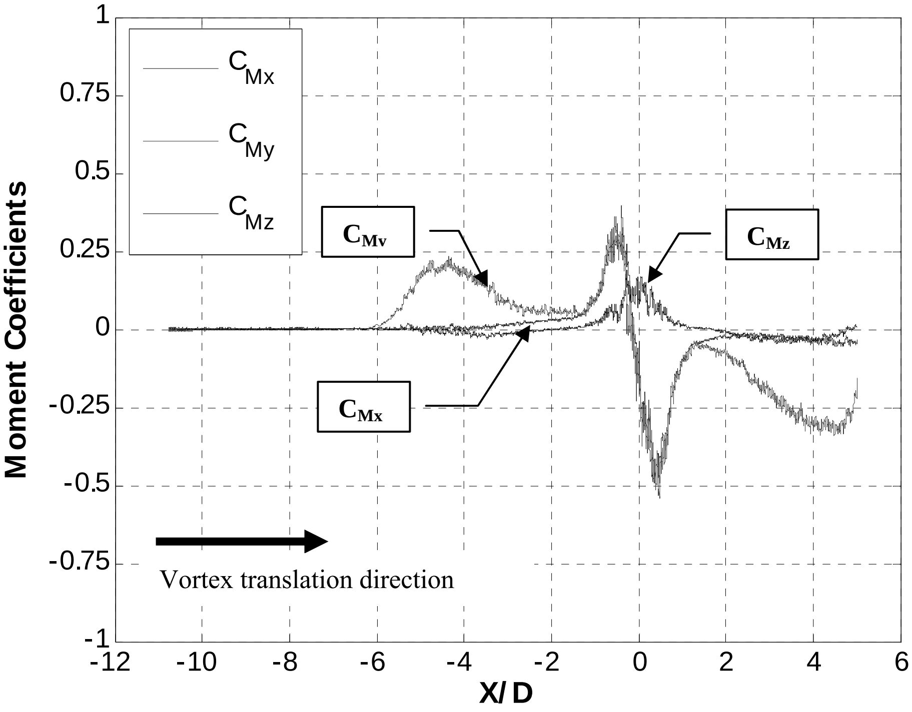

Figure 2-11: Time history of moment coefficients showing relative magnitudes for Case 1

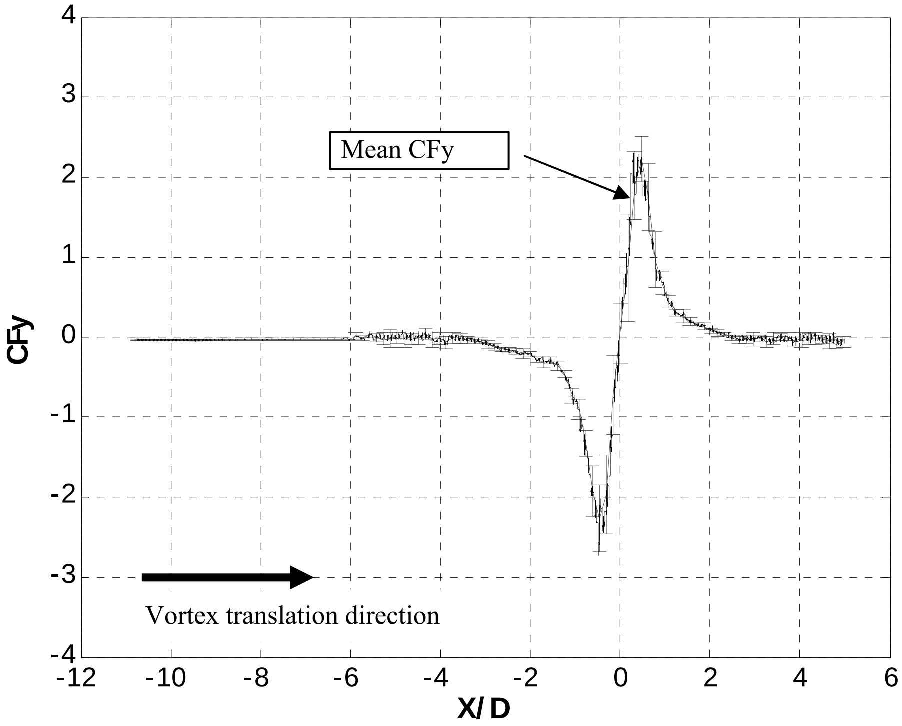

Figure 2-12: Ensemble average C_{F_y} for Case 1 with 95% confidence intervals.

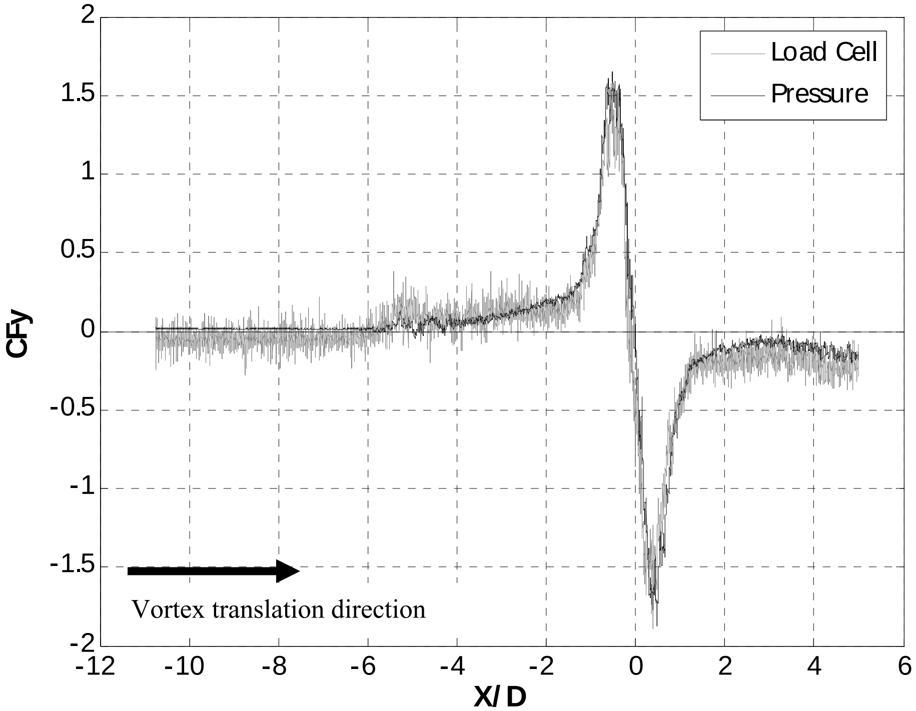

Figure 2-13: C_{F_y} comparison between load cell and pressure data for Case 1

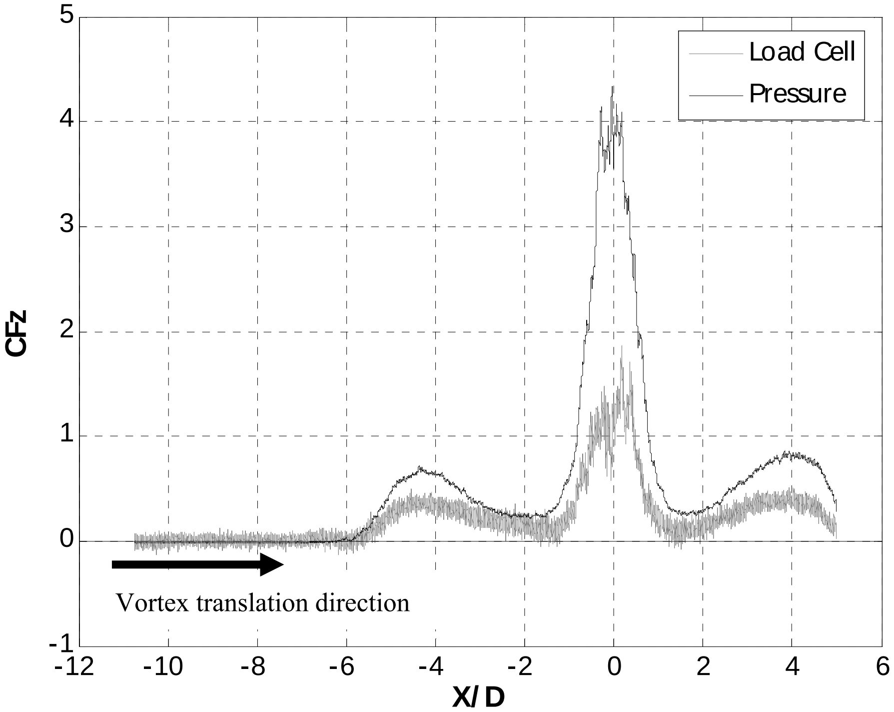

Figure 2-14: C_{F_z} comparison between load cell and pressure data for Case 1

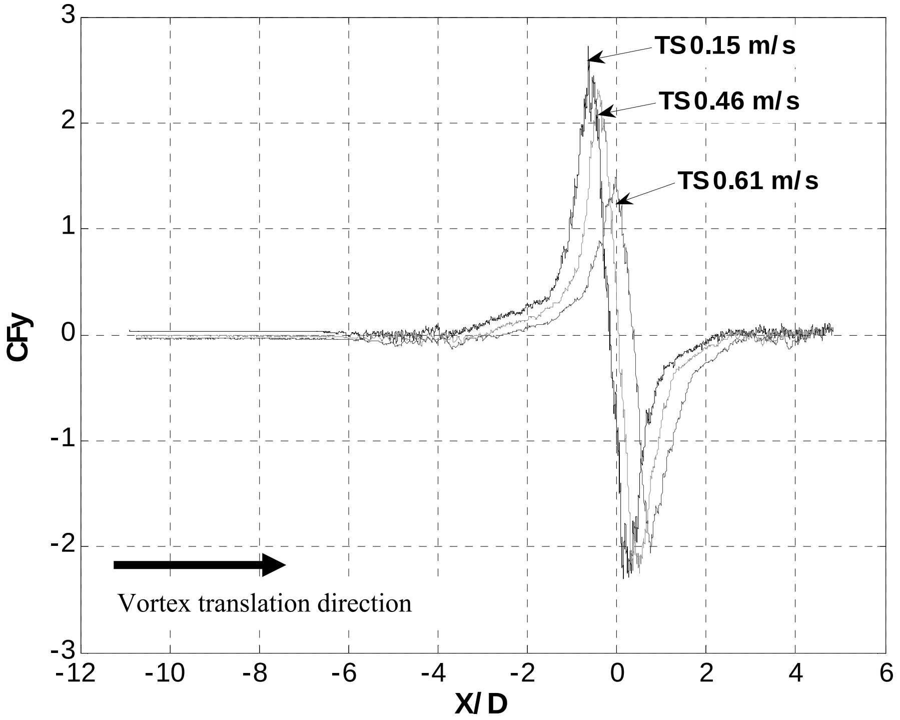

Figure 2-15: C_{F_y} comparison between different vortex translation speeds (TS) for Case 1

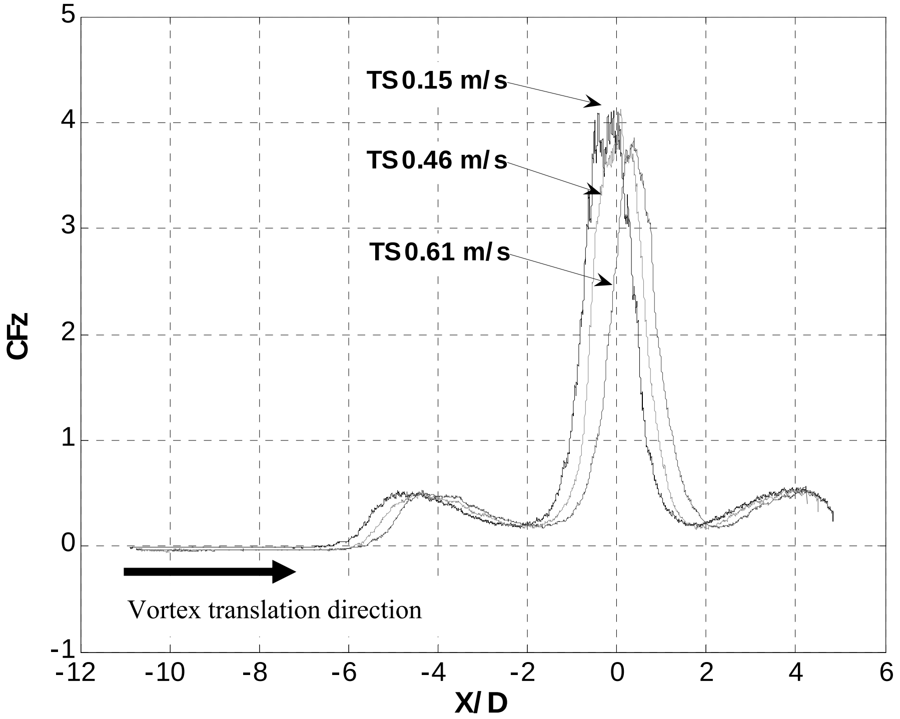

Figure 16: C_{F_z} comparison between different vortex translation speeds for Case 1

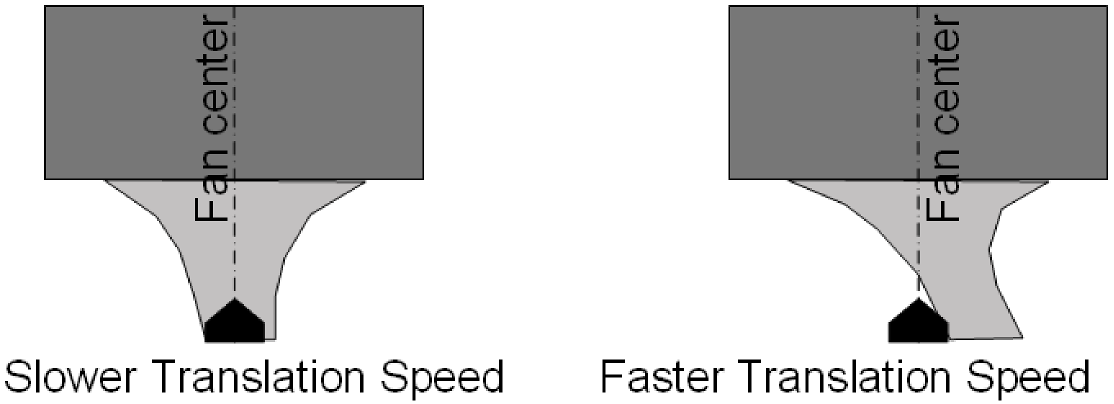

Figure 2-17: Shows the effect of slower and faster vortex translation speed on the model

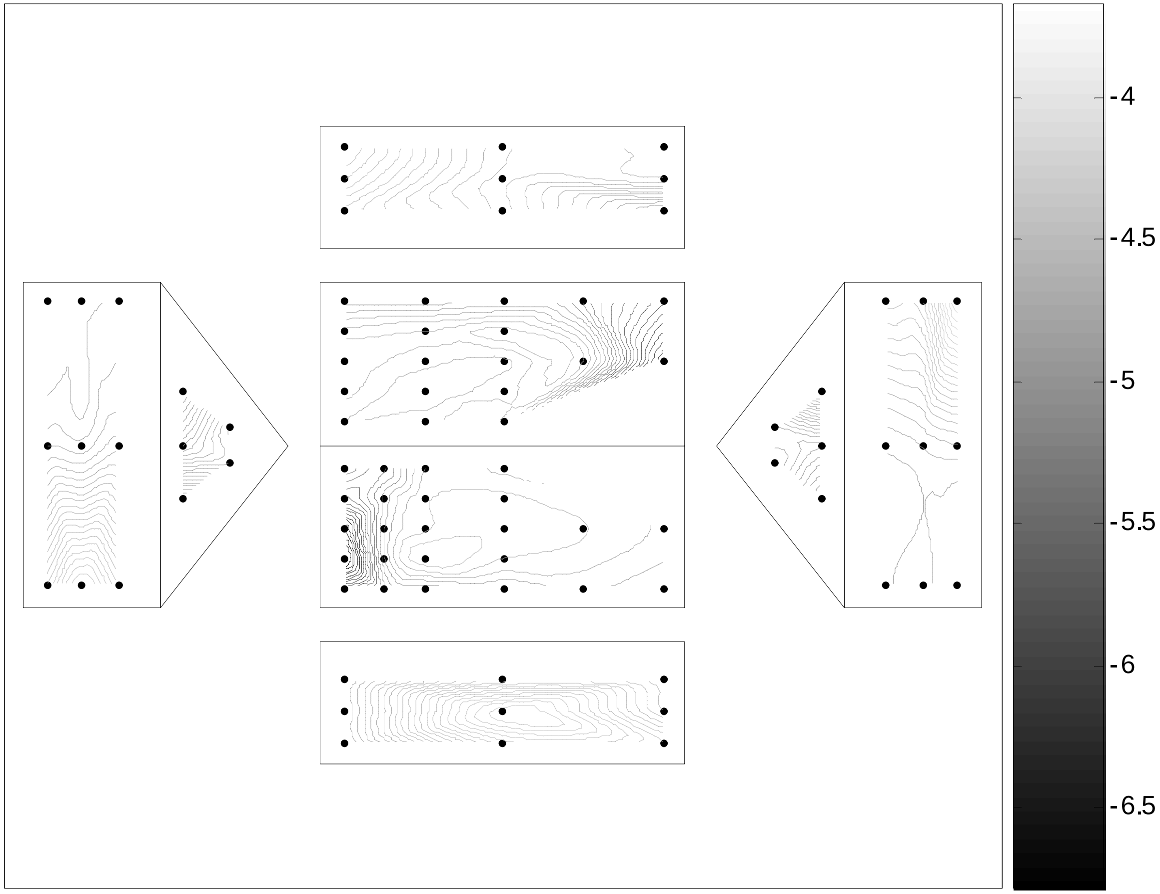

Figure 2-18: Local peak $C_{\hat{p}}$ distribution for Case 17. This case exhibited some of the largest peak force coefficients. The arrow denotes the vortex translation direction.

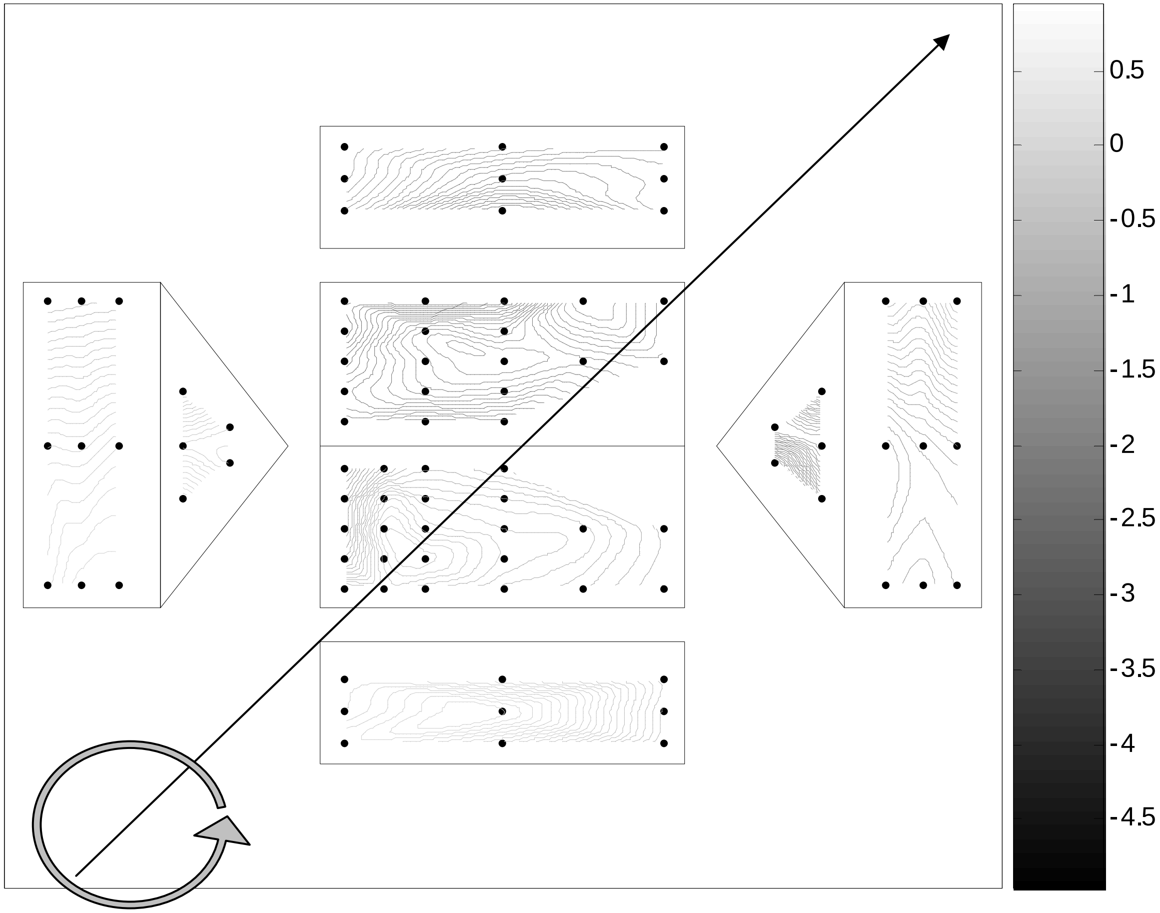

Figure 2-19: Instantaneous C_p distribution for Case 17 corresponding to a tornado position of $x/D = -0.45$. The arrow denotes the vortex translation direction and the rotating vector denotes the position of the tornado vortex not yet at the building.

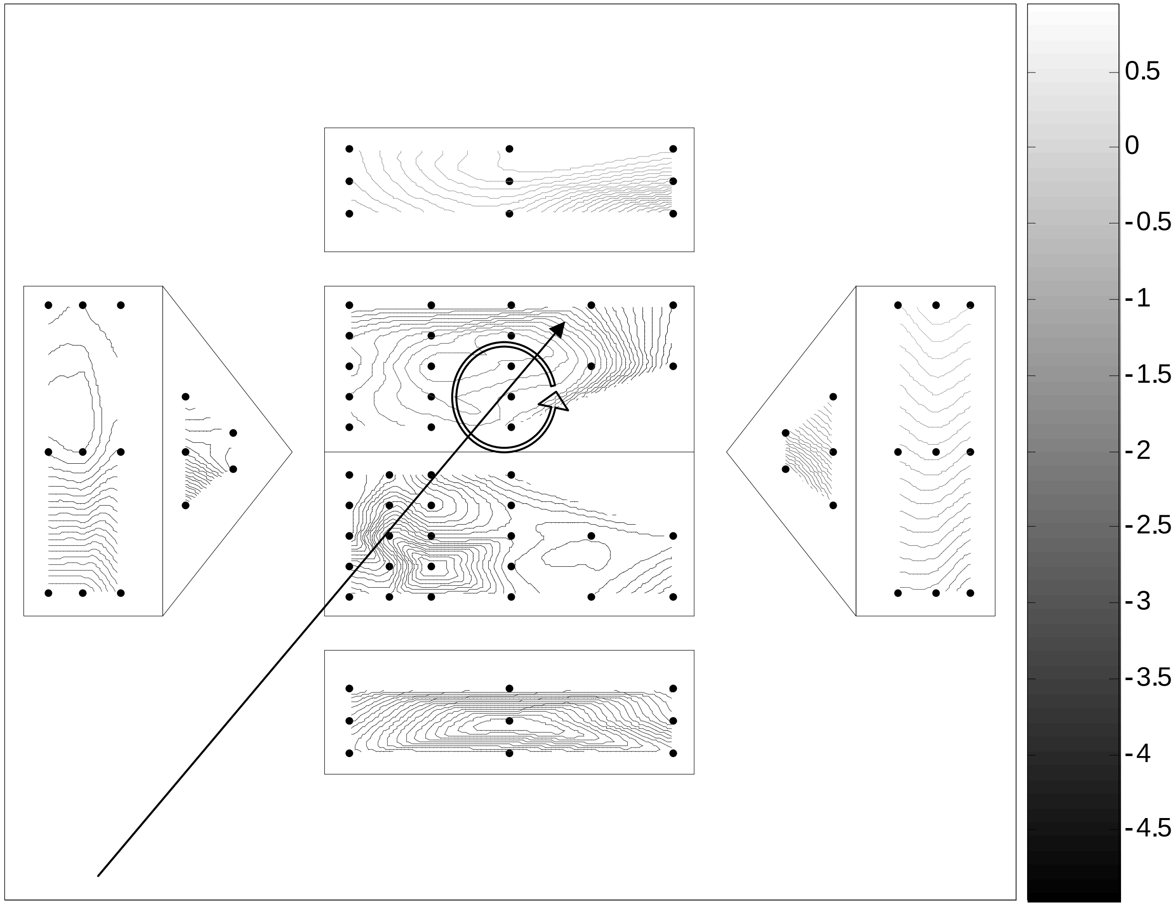

Figure 2-20: Instantaneous C_p distribution for Case 17 corresponding to a tornado position of $x/D = +0.45$. The arrow denotes the vortex translation direction and the rotating vector denotes the position of the tornado vortex after having passed the building.

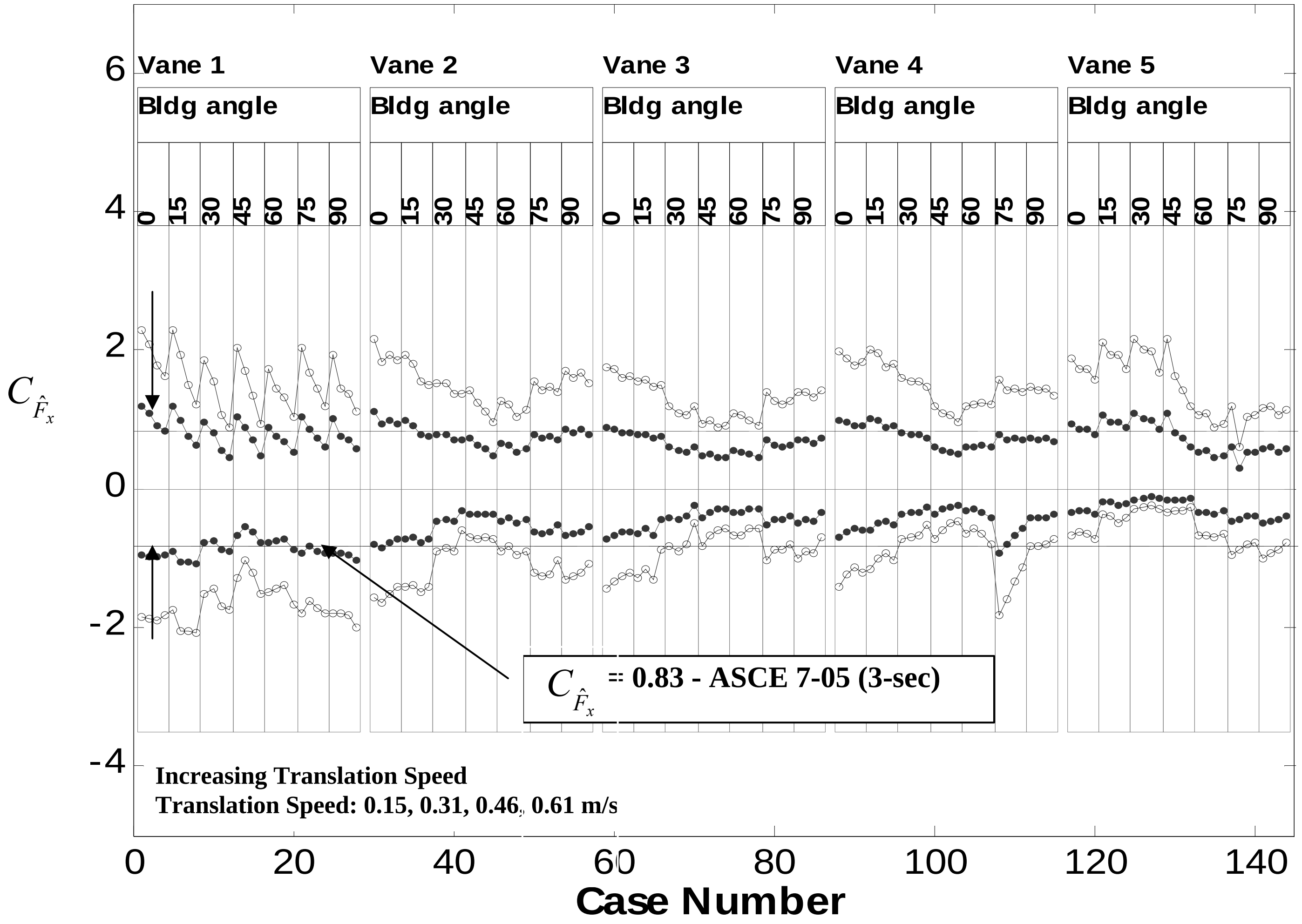

Figure 2-21: Maximum and minimum $C_{\hat{F}_x}$ for gable roof building. Open symbols represent model-scale coefficients; filled symbols represent full-scale coefficients.

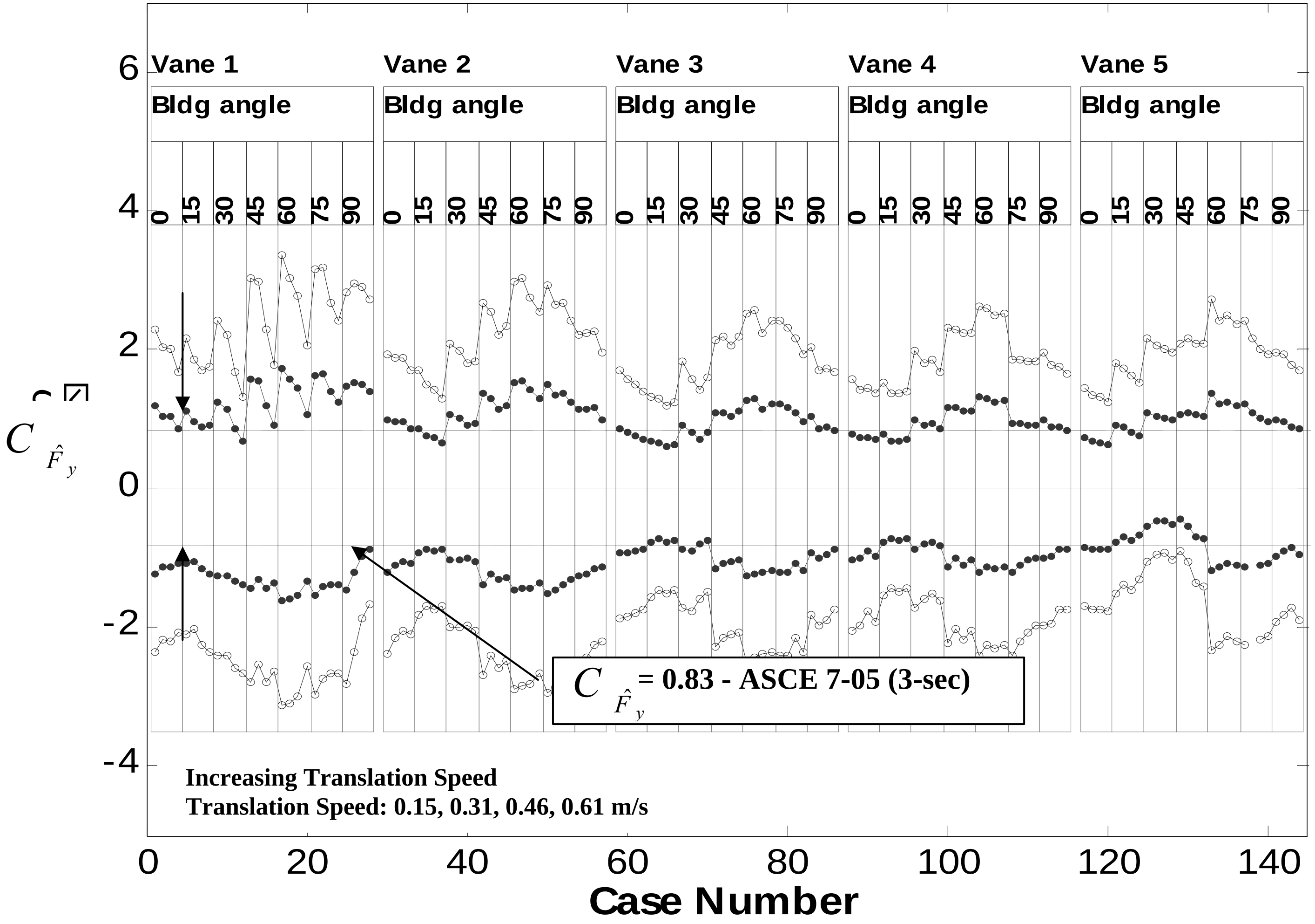

Figure 2-22: Maximum and minimum $C_{\hat{F}_y}$ for gable roof building. Open symbols represent model-scale coefficients; filled symbols represent full-scale coefficients.

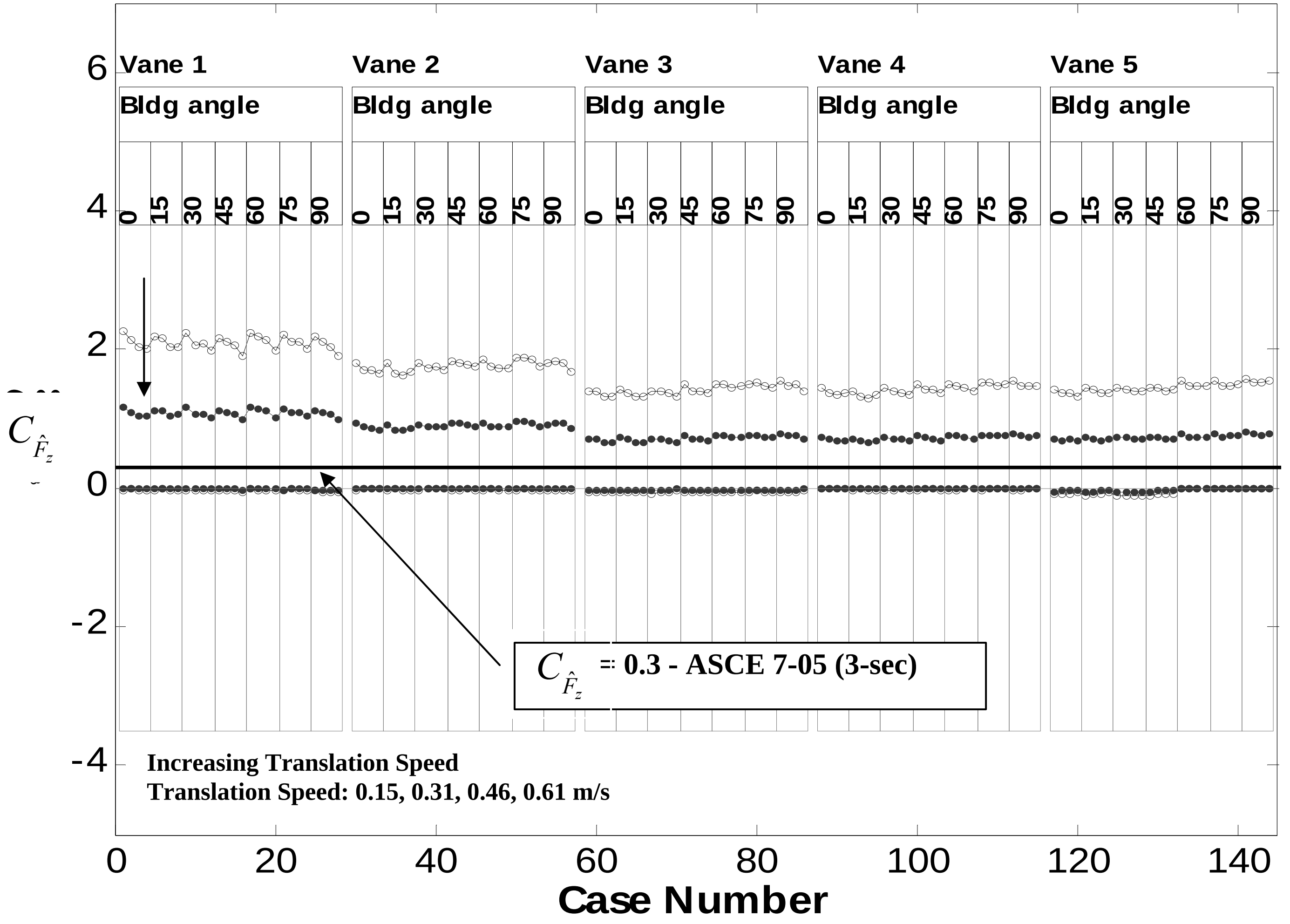

Figure 2-23: Maximum and minimum $C_{\hat{F}_z}$ for gable roof building. Open symbols represent model-scale coefficients; filled symbols represent full-scale coefficients.

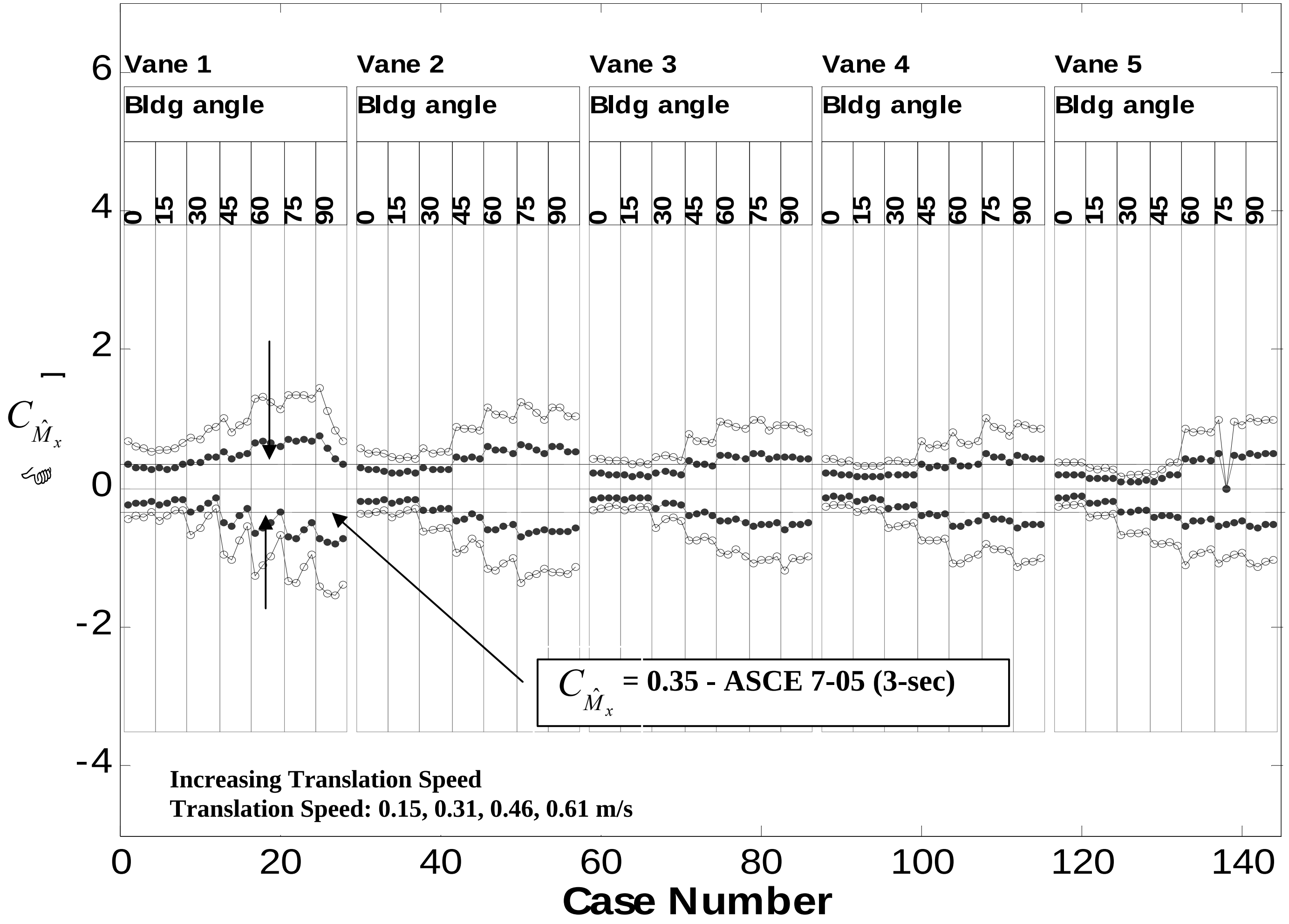

Figure 2-24: Maximum and minimum $C_{\hat{M}_x}$ for gable roof building. Open symbols represent model-scale coefficients; filled symbols represent full-scale coefficients.

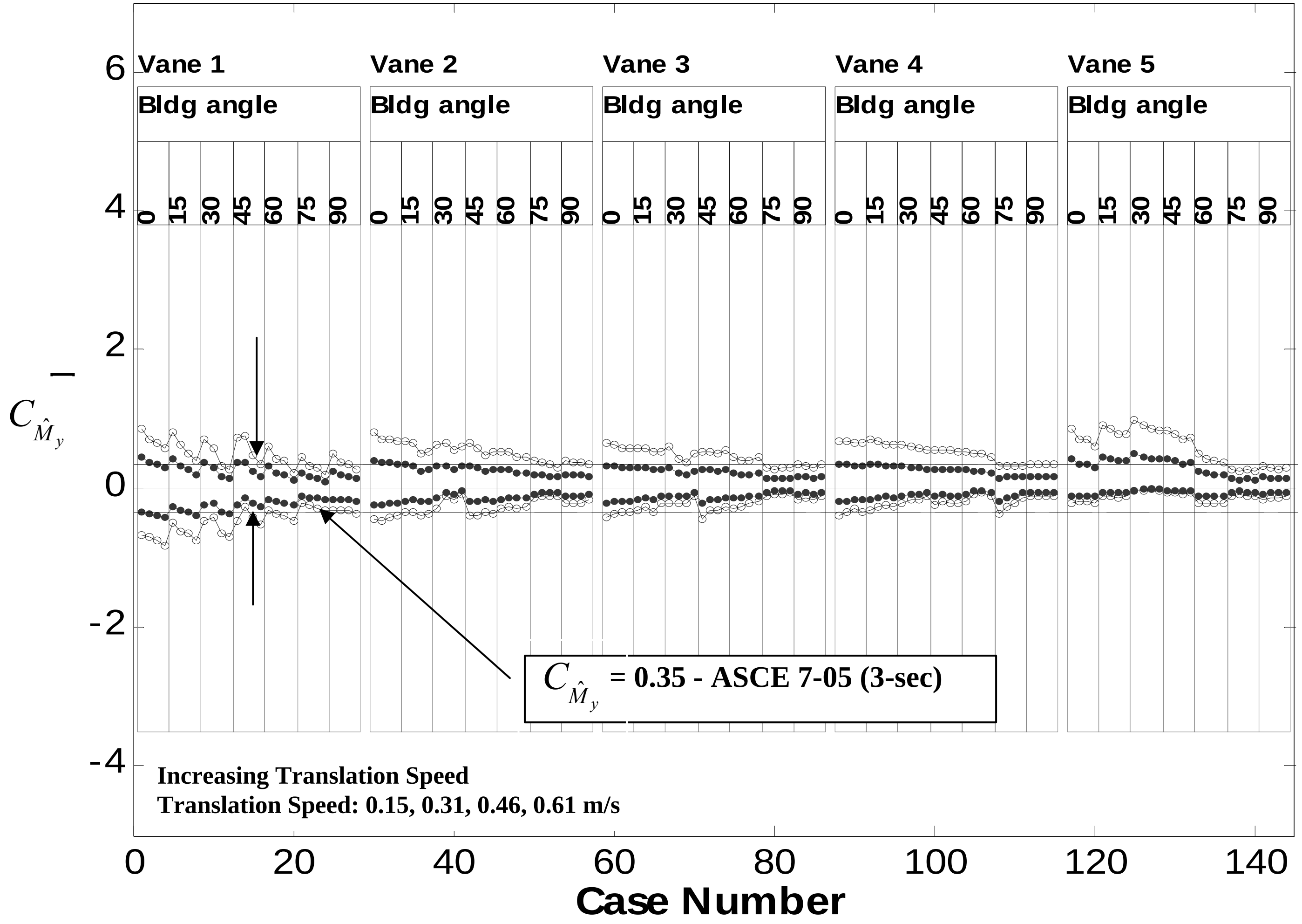

Figure 2-25: Maximum and minimum $C_{\hat{M}_y}$ for gable roof building. Open symbols represent model-scale coefficients; filled symbols represent full-scale coefficients.

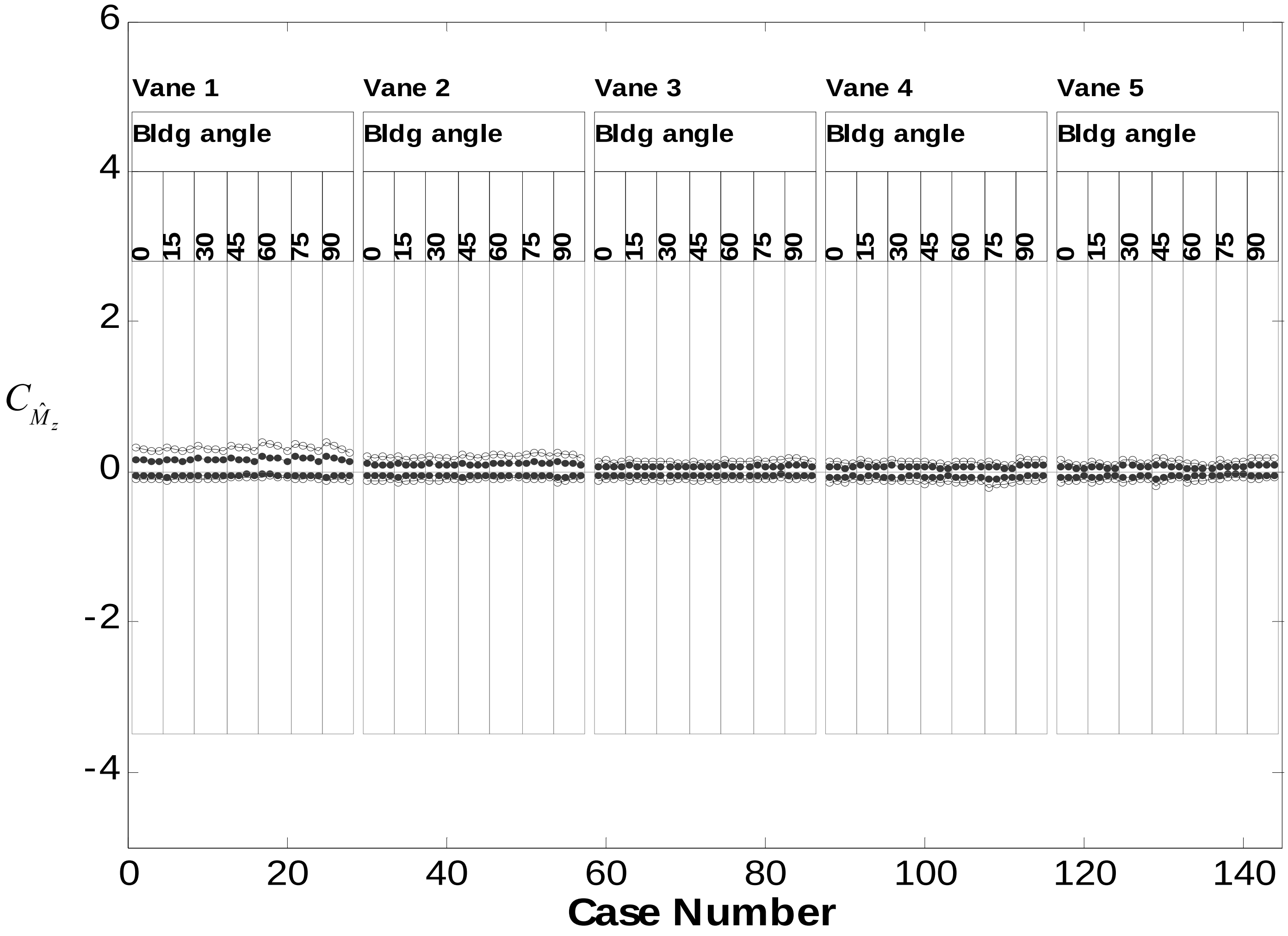

Figure 2-26: Maximum and minimum $C_{\hat{M}_z}$ for gable roof building. Open symbols represent model-scale coefficients; filled symbols represent full-scale coefficients.

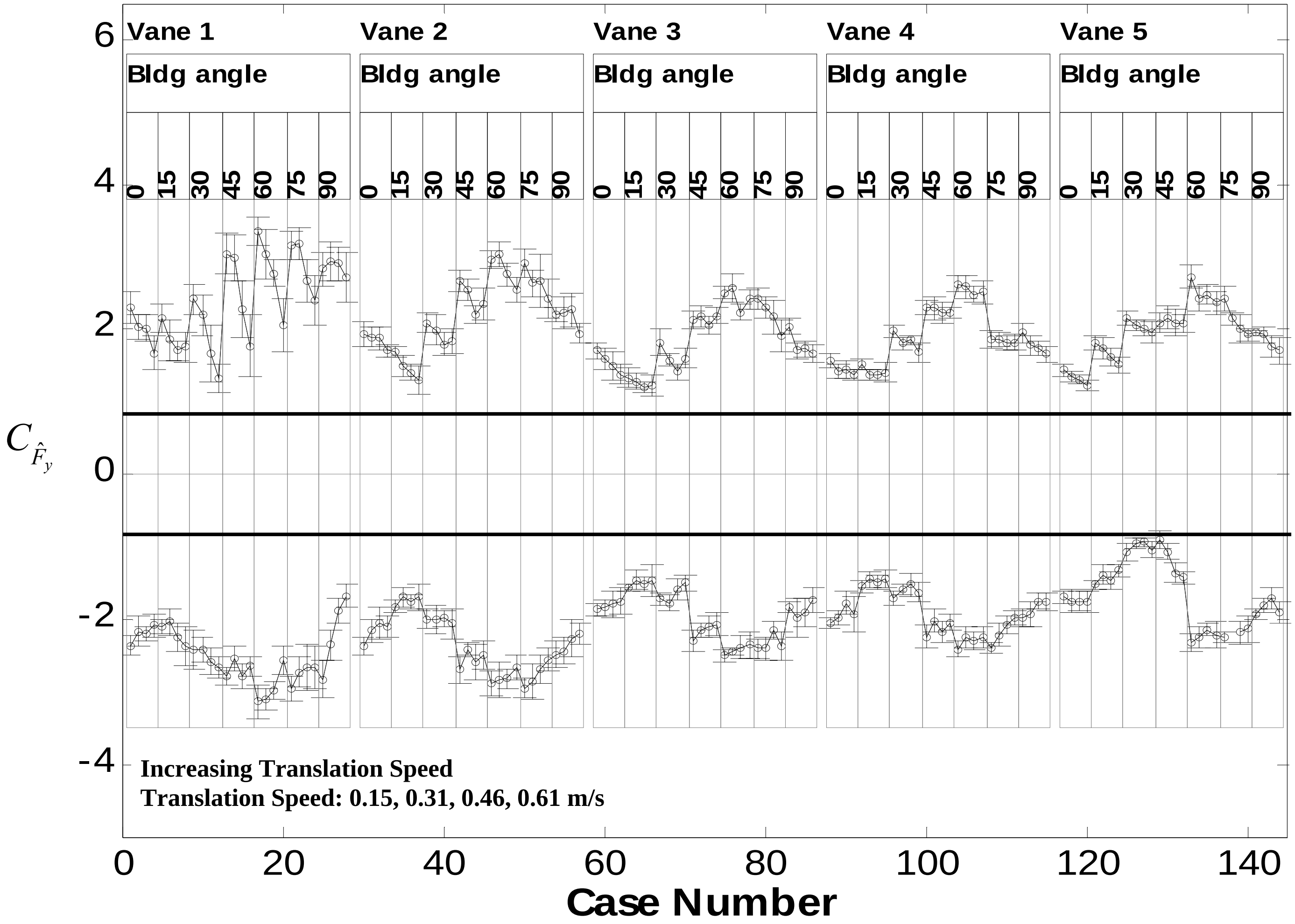

Figure 2-27: Maximum & minimum $C_{\hat{F}_y}$ with 95% confidence interval

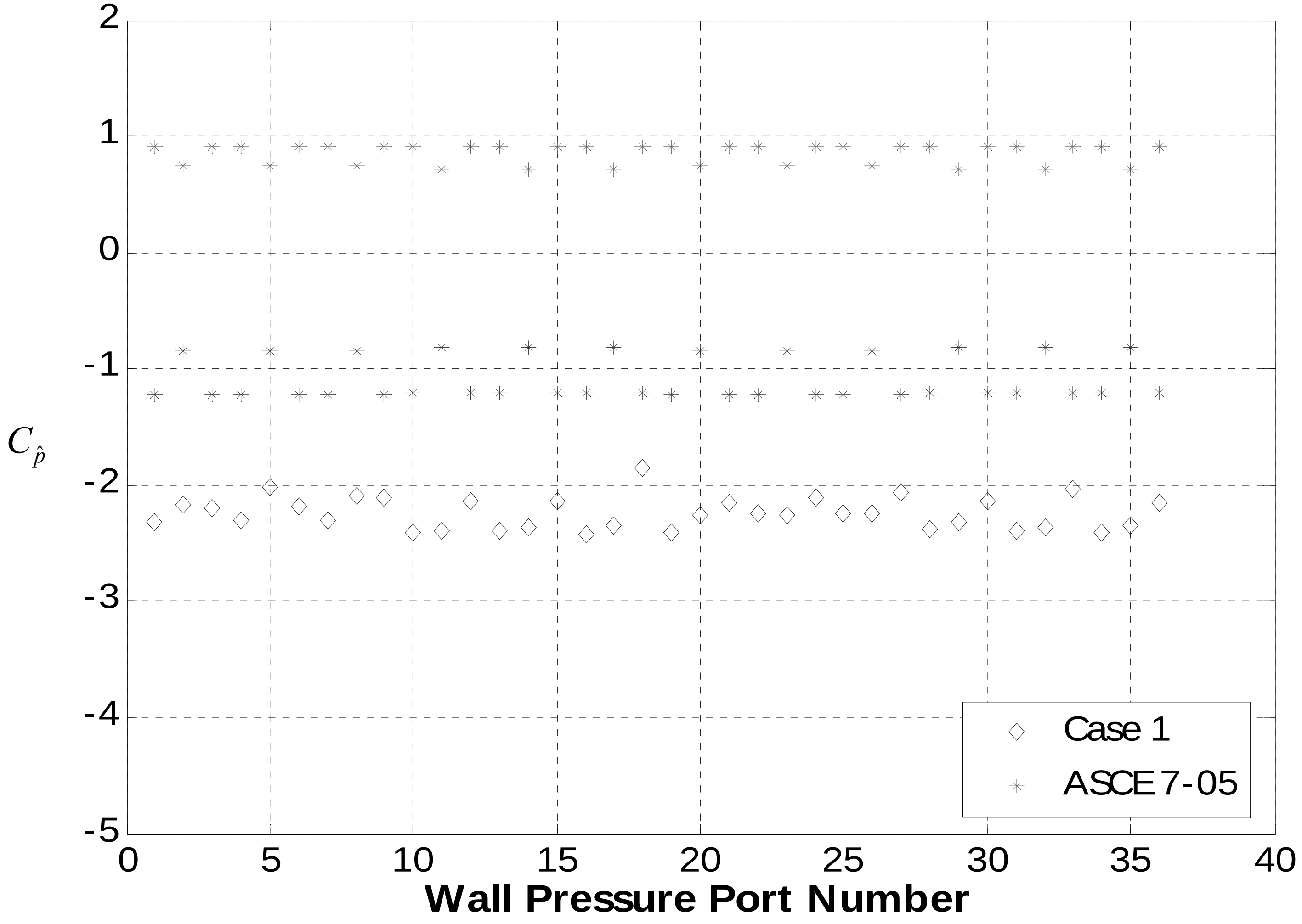

Figure 2-28: Wall $C_{\hat{p}}$ comparison between the worst tornado case and ASCE 7-05

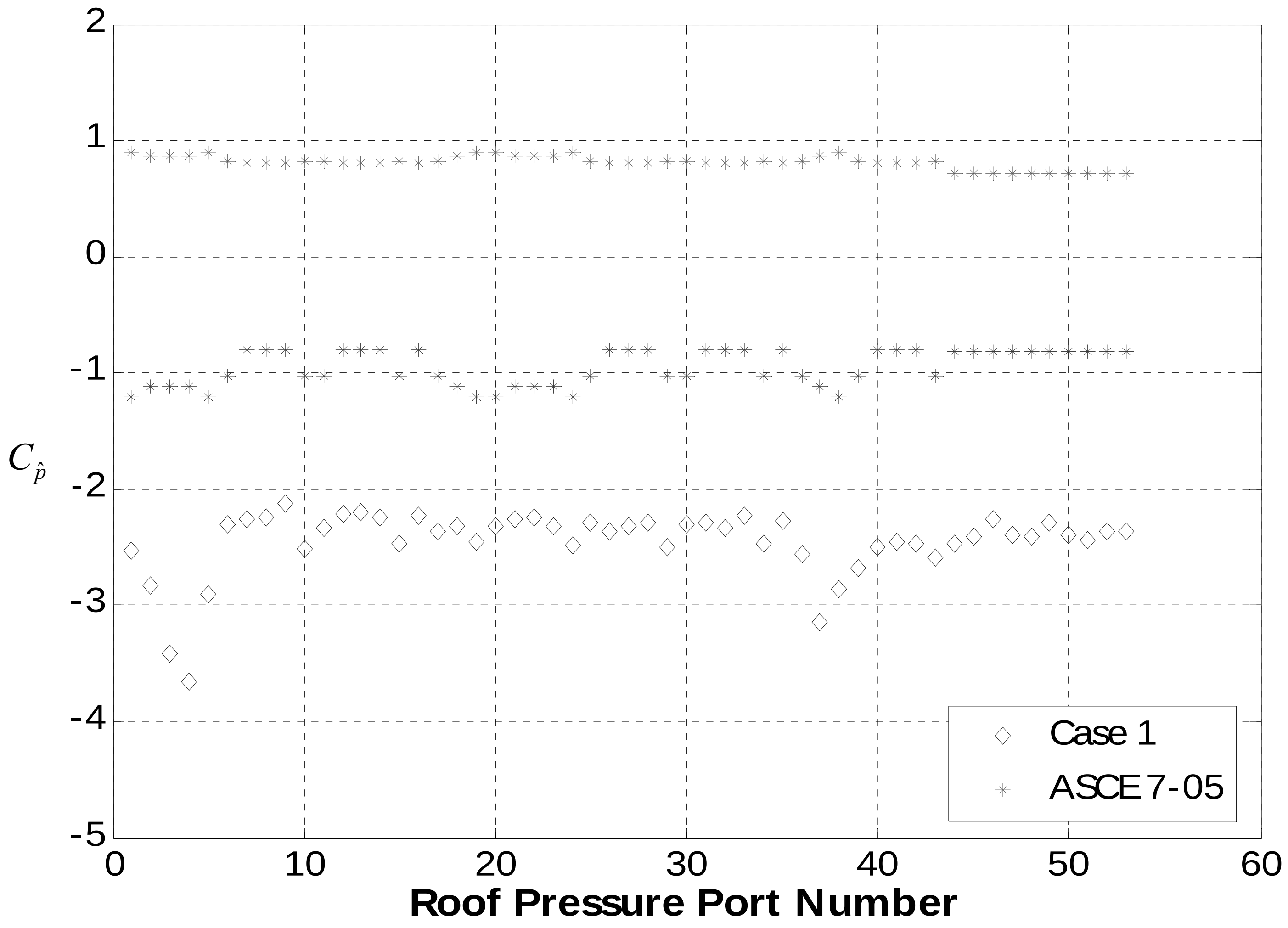

Figure 2-29: Roof $C_{\hat{p}}$ comparison between the worst tornado case and ASCE 7-05. NOTE: $C_{\hat{F}_z}$ from ASCE 7-05 is a combination of positive and negative $C_{\hat{p}}$ values on the roof, whereas for the tornado case $C_{\hat{p}}$ is negative throughout

Case Name	Vane Angle (deg)	Fan Speed (%FS)	Floor Height (m)	S at RMW	RMW (m)	$V_{\theta_{\max}}$ (m/s)	Q ($\mathrm{m^3/s}$)	λ_T	Re $\times 10^4$
Vane1	15	0.33	0.46	0.08	0.23	6.9	14.4	10.4	4.3
Vane2	25	0.33	0.46	0.18	0.30	8.3	13.1	12.5	5.1
Vane3	35	0.33	0.46	0.24	0.30	9.7	11.5	14.7	6.0
Vane4	45	0.33	0.46	0.82	0.51	9.8	9.7	14.9	6.1
Vane5	55	0.33	0.46	1.14	0.53	9.7	7.6	14.8	6.0

Table 2-1: Experimental simulator settings and the accompanying tornado vortex parameters.
S=Swirl Ratio, RMW = Radius of Maximum Wind, Q = Volume Flow Rate, λ_T= Time Scale, Re = Model Reynolds No.

Bldg. Angle	Vane 1				Vane 2				Vane 3				Vane 4				Vane 5			
	TS1	TS2	TS3	TS4	TS1	TS2	TS3	TS4	TS1	TS2	TS3	TS4	TS1	TS2	TS3	TS4	TS1	TS2	TS3	TS4
0	**1***	**2***	3	**4***	29	30	31	32	57	58	59	60	85	86	87	88	113	114	115	116
15	5	6	7	8	33	34	35	36	61	62	63	64	89	90	91	92	117	118	119	120
30	9	10	11	12	37	38	39	40	65	66	67	68	93	94	95	96	121	122	123	124
45	**13***	**14***	15	**16***	41	42	43	44	69	70	71	72	97	98	99	100	125	126	127	128
60	17	18	19	20	45	46	47	48	73	74	75	76	101	102	103	104	129	130	131	132
75	21	22	23	24	49	50	51	52	77	78	79	80	105	106	107	108	133	134	135	136
90	25	26	27	28	53	54	55	56	81	82	83	84	109	110	111	112	137	138	139	140

Table 2-2: Test matrix for the building tests including 5 tornado simulator vane angles and 7 building orientation angles. All case numbers (1-140) listed corresponds to pressure measurements and * corresponds to the force measurements (FM - for validation only) carried out for those test points. All the above cases involved 10 repeat runs each.

References

M. Allaby (2004) *Dangerous Weather – Tornadoes*, Rev. Ed., New York: Facts on File, 57-62

Bienkiewicz, B., Dudhia, P. (1993). “Physical Modeling of Tornado-Like Flow and Tornado Effects on Building Loading.” *Proc. Seventh U.S. National Conference on Wind Engineering* 95-106.

Bluestein, H.B., Golden, J. (1993). “A review of tornado observations.” in Church, Burgess, Doswell, Davies- Jones, Eds., *The tornado: Its structure, dynamics, prediction, and hazards, American Geo*. Mon. 79,

Brooks, H. E., and Doswell III, C. A. (2001). “Normalized damage from major tornadoes in the United States: 1890-1999.” *Wea. Forecasting*, 16(1), 168–176.

Chang, C.C. (1971). “Tornado effects on buildings and structures with laboratory Simulation.” *Proc. Third International Conference on Wind Effects on Buildings and Structures*, Tokyo, Japan 231-240.

Church, C.R., Snow, J. T., Baker, G. L., Agee, E. M. (1979). “Characteristics of tornado-like vortices as a function of swirl ratio: A laboratory investigation.” *J. Atmos. Sci.,36,* 1755-1776.

Davies-Jones, R.P. (1976). “Laboratory Simulation of Tornadoes.” *Proceedings of the Symposium on Tornadoes, Assessment of Knowledge and Implications for Man, Ed. R.E. Peterson, Texas Tech University*, 151-174.

Doswell III, C.A., Edwards, R., Thompson, R.L., Hart, J.A., Crosbie, K.C. (2006). “A simple and flexible method for ranking severe weather events.” *Wea. Forecasting*, 21(6), 939–951.

Forbes, G. (2006). “Meteorological aspects of high-impact tornado outbreaks.” *Extended Abstracts, Symp. on the Challenges of Severe Convective Storms*, AMS, Atlanta, GA (CD-ROM) P1.12.

Fouts, L., James, D.L., and Letchford, C.W. (2003). “Pressure Distribution on a Cubical Model in Tornado-Like Flow.” *Proceedings of the10th International Wind Engineering Conference*, Lubbock, TX..

Haan, Jr., F.L., Sarkar, P.P., Gallus, W.A. (2007) “Design, construction and performance of a large tornado simulator for wind engineering applications.” *Engineering Structures*, in press.

Jischke, M. C., Light, B. D. (1983). “Laboratory simulation of tornadic wind loads on a rectangular model structure.” *Proc. Sixth International Conference on Wind Engineering*, Australia & New Zealand, v. 1

Mishra, A.R., James, D.L. and Letchford, C.W. (2005). “Comparison of Pressure Distribution on a Cubical Model in Boundary Layer and Tornado-Like Flow Fields.” *Proceedings of the Tenth Americas Conference on Wind Engineering*. Baton Rouge, LA. 2005.

Sarkar P.P., Haan F.L., Balaramudu V. and Sengupta A. (2006). “Laboratory simulation of tornado and microburst to assess wind loads on buildings.” *Proc., ASCE Structures Congress*, ASCE, Reston, VA.

Sengupta A., Haan F.L., Sarkar P.P. and Balaramudu V. (2007). “Transient loads on buildings in microburst and tornado winds.”Accepted for publication in *Journal of Wind Engineering and Industrial Aerodynamics*.

Speheger, D.A., Doswell III, C.A., Stumpf, G.J. (2002). “The tornadoes of 3 May 1999: Event verification in central Oklahoma and related issues.” *Wea. Forecasting.*, 17(3), 362–381.

Ward, N.B. (1972). “The exploration of certain features of tornado dynamics using a laboratory model.” *J. of the Atmospheric Sciences*, 29, 1194-1204.

Wind Hazard Reduction Coalition, Date Accessed: Jan. 31, 2006
<http://www.windhazards.org>

Wurman, J., Gill, S. (2000). “Fine scale radar observations of the Dimmitt, Texas” (2 June 1995) tornado.” *AMS Monthly Weather Review*, v. 128, 2135-2164.

Wurman, J., Alexander, C.R. (2005). “The 30 May 1998 Spencer, South Dakota, storm. Part II: Comparison of observed damage and radar-derived winds in the tornadoes.” *AMS Monthly Weather Review*, v. 133, 97-118.

Wurman, J., Alexander, C., Robinson, P., Richardson, Y. (2007). “Low-Level Winds in Tornadoes and Potential Catastrophic Tornado Impacts in Urban Areas.” *Bull. Amer. Met. Soc.*, 88(1), 31-46.

Wurman, J., Personal Communication (2004).

Wurman, J., Personal Communication (2005).

CHAPTER 3. DIFFERENT BUILDING MODELS

3.1 Introduction

This section presents the results and discussion for the different low-rise building models. The building models vary in terms of roof shape (1-Flat, 1-Hip and 1, 2, 3-Gable roofs) and floor height (1, 2 Story). In the previous section a particular gable roof model (35^o roof) with floor height of 1 story was tested under five different vortex structures (Vane 1 to Vane 5). The results from that case clearly showed higher loads occurring for Vane 1, which corresponds to the tornado with smaller core radius. Hence, for the present analysis all the different building models were tested under the tornado with smaller core radius (Vane 1). This enables us to understand the behavior of the wind loadings on the various low-rise building models for the same condition. The models were tested for 3 different building orientations (0^o, 45^o and 90^o deg) and 3 different vortex translation speeds (0.15, 0.46 and 0.61 m/s). The details of the models, test setup and results are discussed in the following section.

3.2 Pressure Model Description

The pressure models are designed for 1:100 scale. The building model roofs (5 No.) and the base (2 No.) are modular in nature, so that different building models can be constructed by combining a particular roof and a base. The model was constructed with plexiglass surface and contains pressure taps to measure the overall external pressure distribution. The surface pressures were measured using a high speed electronic pressure scanner. The complete description of the model dimensions are listed in Table 3.1. The various low-rise building models are shown from Figure 3.1 to Figure 3.10.

3.3 Pressure Instrumentation

The same high speed electronic pressure scanners (Scanivalve ZOC33/64Px) described in the previous chapter were used to measure the surface pressures for these building models. The vinyl tubing used to connect the pressure taps to the sensor was 15 inch in length. The static pressure for all pressure measurements was the laboratory ambient pressure outside the tornado simulator. The pressure transducer was zero calibrated before the start of the measurement using standard calibration technique recommended by the manufacturer. The pressure signals were corrected off-line for the dynamic effects of the tubing. Data were sampled at the rate of 430 Hz (controlled by an external clock). The initiation of data acquisition and the crane movement were synchronized using a common external trigger. The test matrix is given in Table 3.1

3.4 Results and Discussion

The force and moment data were obtained by integrating the surface pressures. The objective of the present analysis is to find the changes in the loading pattern due to the geometric variation of the buildings. Therefore, the results are not compared with the building code estimates. For this reason, the coefficients obtained by normalizing the force and moment data using the model scale values are not scaled for the full-scale conditions. Further, the ratios of the coefficients for 1 & 2 story building models will be the same irrespective of the model or full-scale analysis.

The following equation is used for normalizing the force and moment, the S, S_z are the projected areas of the respective building models in the windward direction (when the model is in 0^{o} deg orientation).

$$
\begin{aligned}
C_{F_x} &= \frac{F_x}{\frac{1}{2}\rho V_{\theta_{\max}}^2 S} & C_{M_x} &= \frac{M_x}{\frac{1}{2}\rho V_{\theta_{\max}}^2 Sh} \\
C_{F_y} &= \frac{F_y}{\frac{1}{2}\rho V_{\theta_{\max}}^2 S} & C_{M_y} &= \frac{M_y}{\frac{1}{2}\rho V_{\theta_{\max}}^2 Sh} \qquad (7) \\
C_{F_z} &= \frac{F_z}{\frac{1}{2}\rho V_{\theta_{\max}}^2 S_z} & C_{M_z} &= \frac{M_z}{\frac{1}{2}\rho V_{\theta_{\max}}^2 S_z b}
\end{aligned}
$$

The force and moment coefficients for one & two story building with various roof types are plotted in figure 3-11 to 3-16.

The C_{F_x} comparison plotted in figure 3-11 clearly shows some change in the C_{F_x} component due the building heights and roof shapes. The 1 story flat roof varies from 0.64 to 1.43 times the 2 story flat roof. The hip roof varies from 0.72 to 1.15. On the whole the gable roof models vary from 0.54 to 1.4.

The side force coefficient C_{F_y} shows appreciable change due the height of the model. The flat roof model varies from 0.57 to 1.02. For the hip roof the 1 floor case is lower by 0.49 to 0.83. The 1 floor gable roofs vary from 0.4 to 1.1 times the 2 floor gable roof. Overall the side force coefficient is lower for 1 story case.

The uplift force coefficient C_{F_z} comparison plotted in figure 3-13 shows little or no change in the values. This clearly states that the uplift force generated by the vortex does not change for different roof shapes and different building heights. The uplift force is generated mainly due to the suction caused by the vortex rather than the aerodynamics of the roof.

The flat roof case shows large variation in the both C_{M_x} and C_{M_y} components. It varies from 0.93 to 2.0 in C_{M_x} and 0.6 to 2.0 in C_{M_y}. The hip roof varies from 0.73 to 1.3 and 0.4 to 1.3 in these moment components. The gable roofs vary from 0.6 to 1.3 and 0.5 to 1.9.

The twisting moment varies roughly 2.3 times for all the building cases.

3.5 Conclusion

The flat roof and gable roof s show the effect of height in the C_{F_x} component. The hip roof shows little change. The Side force C_{F_y} shows appreciable change irrespective of the roof types. The uplift force C_{F_z} does not change. It remains fairly constant for all the roof types and height variations. The C_{M_x} and C_{M_y} coefficients variation is higher for flat roof, followed by gable and hip roof. The twisting moment is consistently higher for the 2 story case.

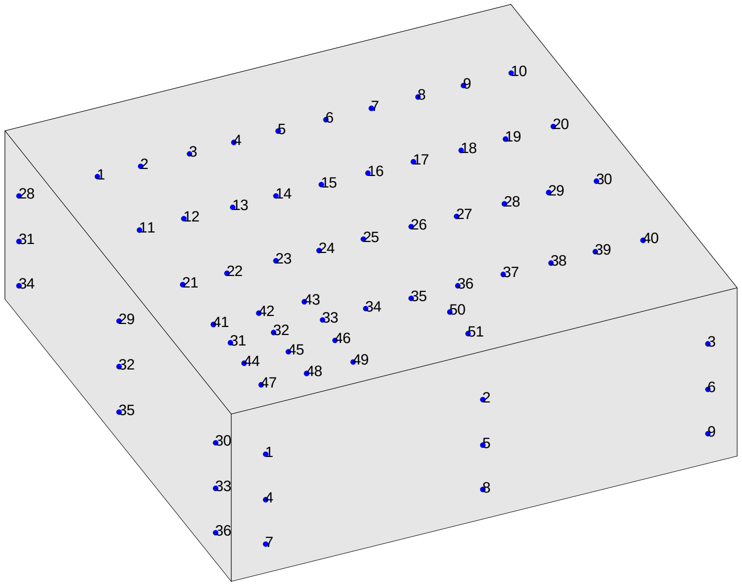

Figure 3-1: 1 Story Flat Roof Model with pressure tap locations

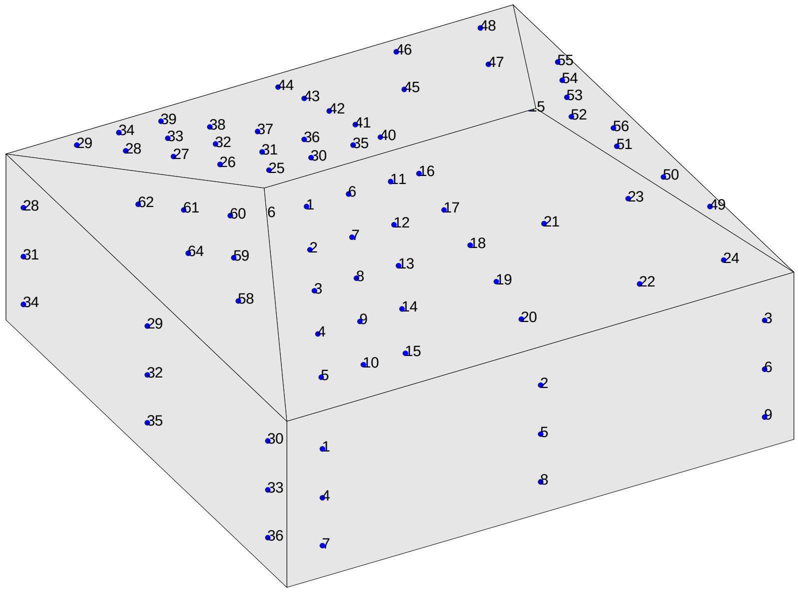

Figure 3-2: 1 Story Hip Roof with θ = 14.5^0 Model with pressure tap locations

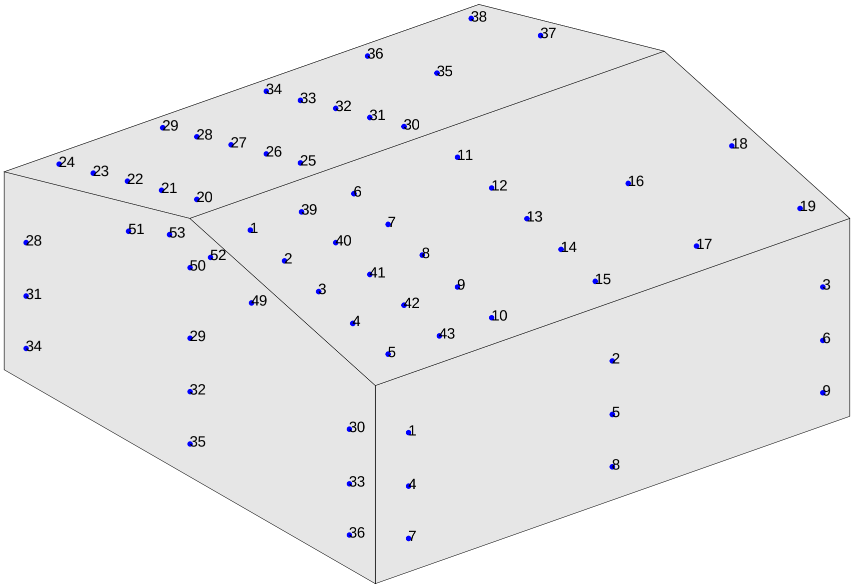

Figure 3-3: 1 Story Gable Roof with θ = 13.4^0 Model with pressure tap locations

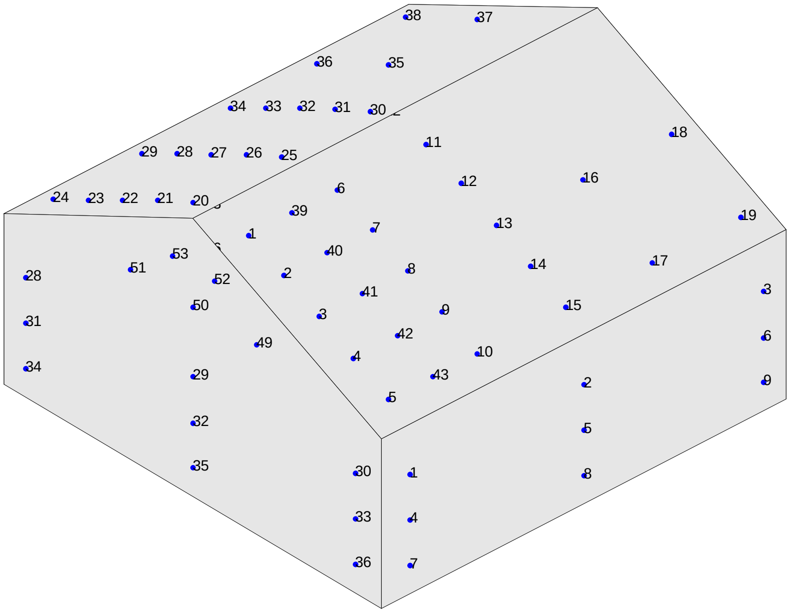

Figure 3-4: 1 Story Gable Roof with θ = 25.5^0 Model with pressure tap locations

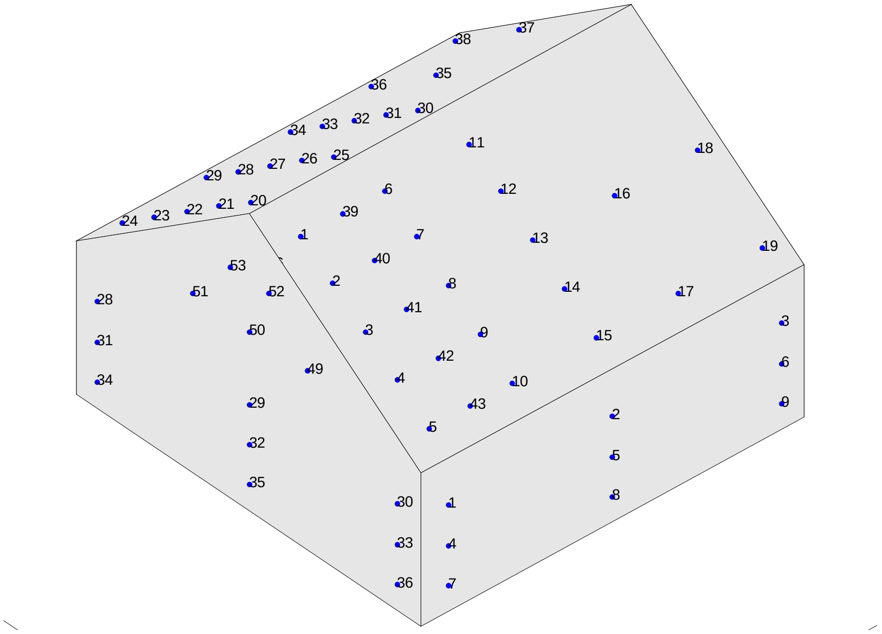

Figure 3-5: 1 Story Gable Roof with $\theta = 35.1^0$ Model with pressure tap locations

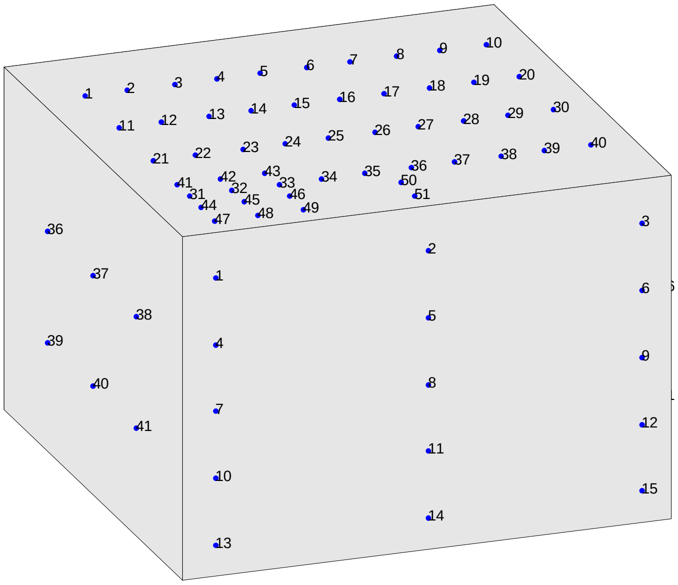

Figure 3-6: 2 Story Flat Roof Model with pressure tap locations

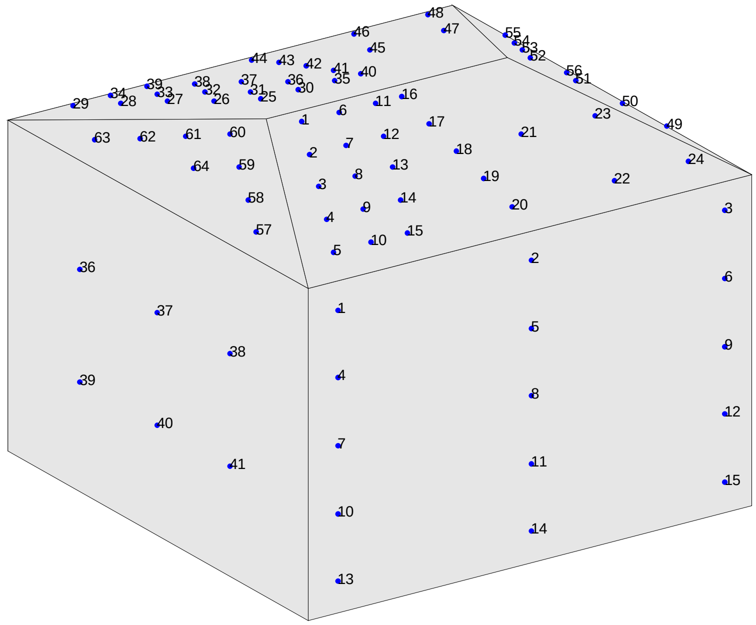

Figure 3-7: 2 Story Hip Roof with θ = 14.5^0 Model with pressure tap locations

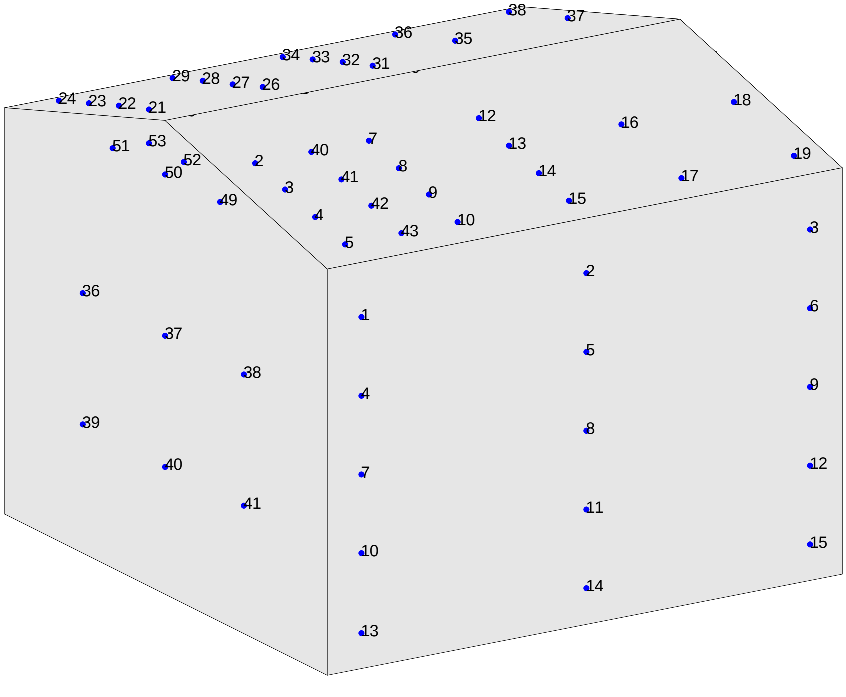

Figure 3-8: 2 Story Gable Roof with θ = 13.4^0 Model with pressure tap locations

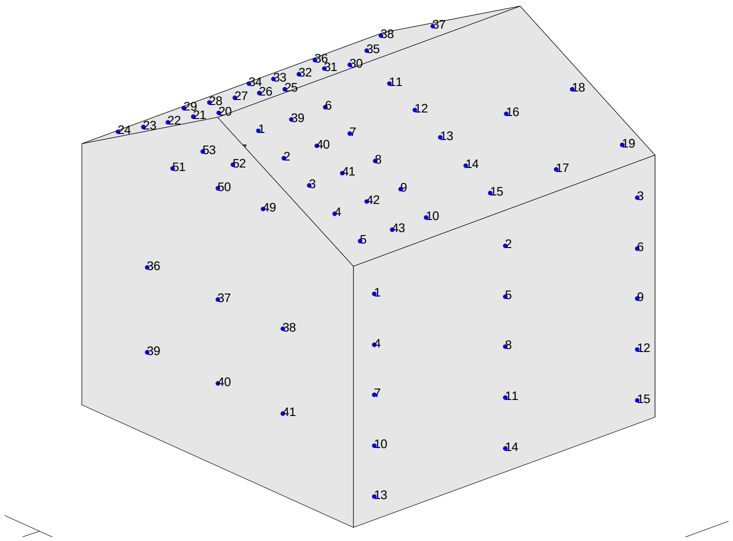

Figure 3-9: 2 Story Gable Roof with θ = 25.5^0 Model with pressure tap locations

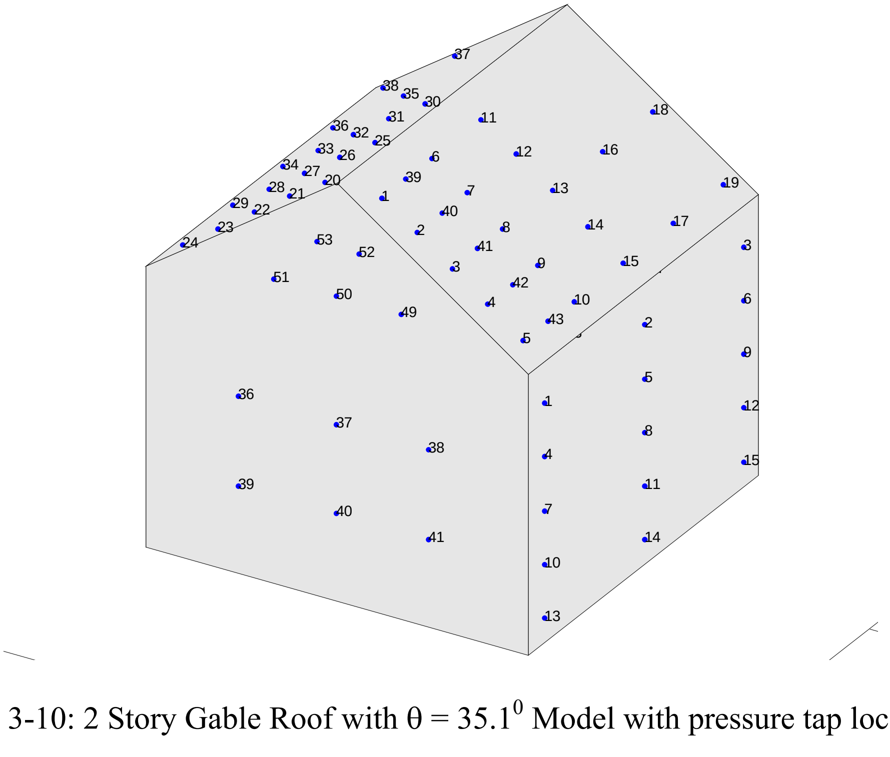

Figure 3-10: 2 Story Gable Roof with θ = 35.1^0 Model with pressure tap locations

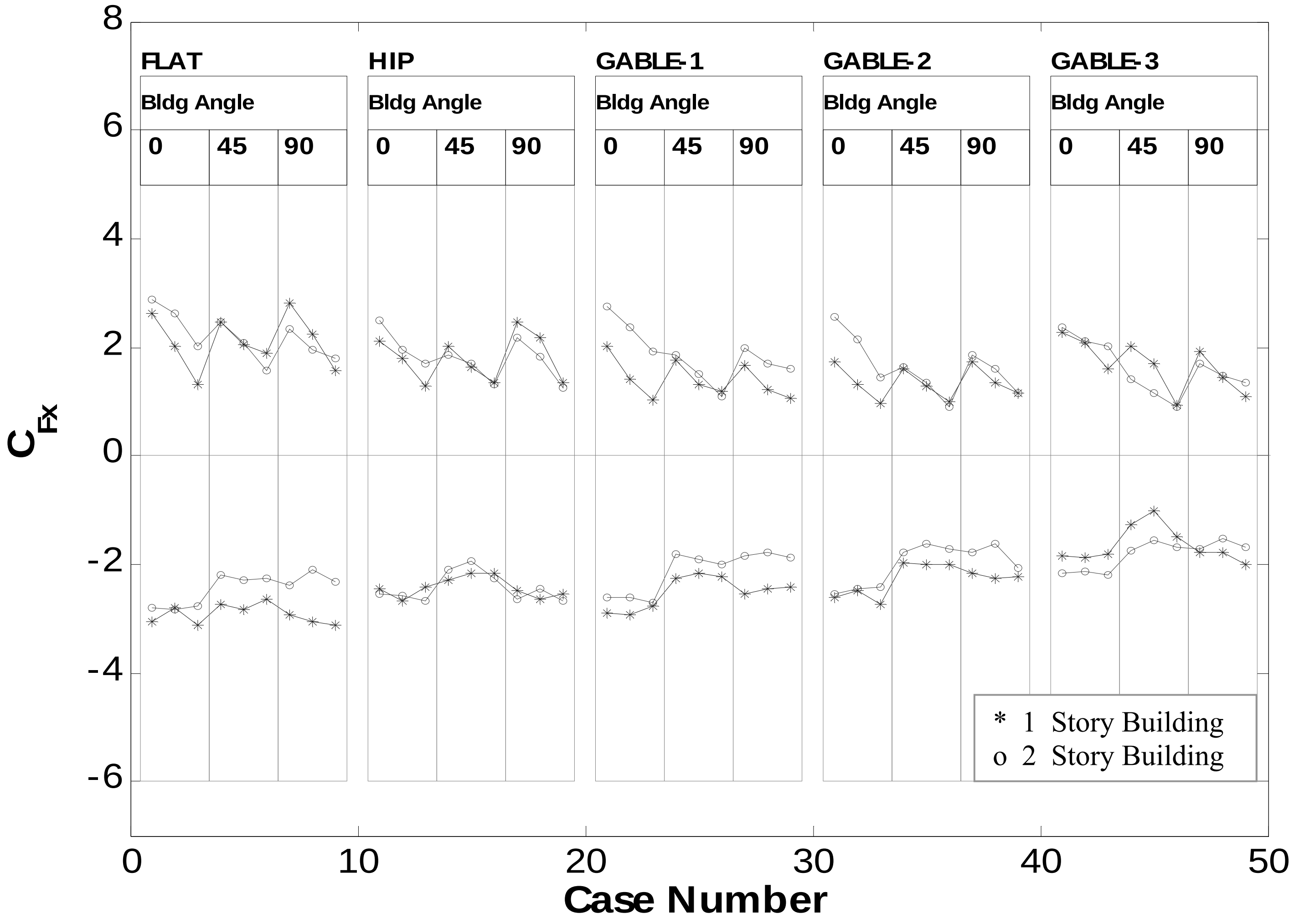

Figure 3-11: Maximum and minimum C_{Fx} for different building models

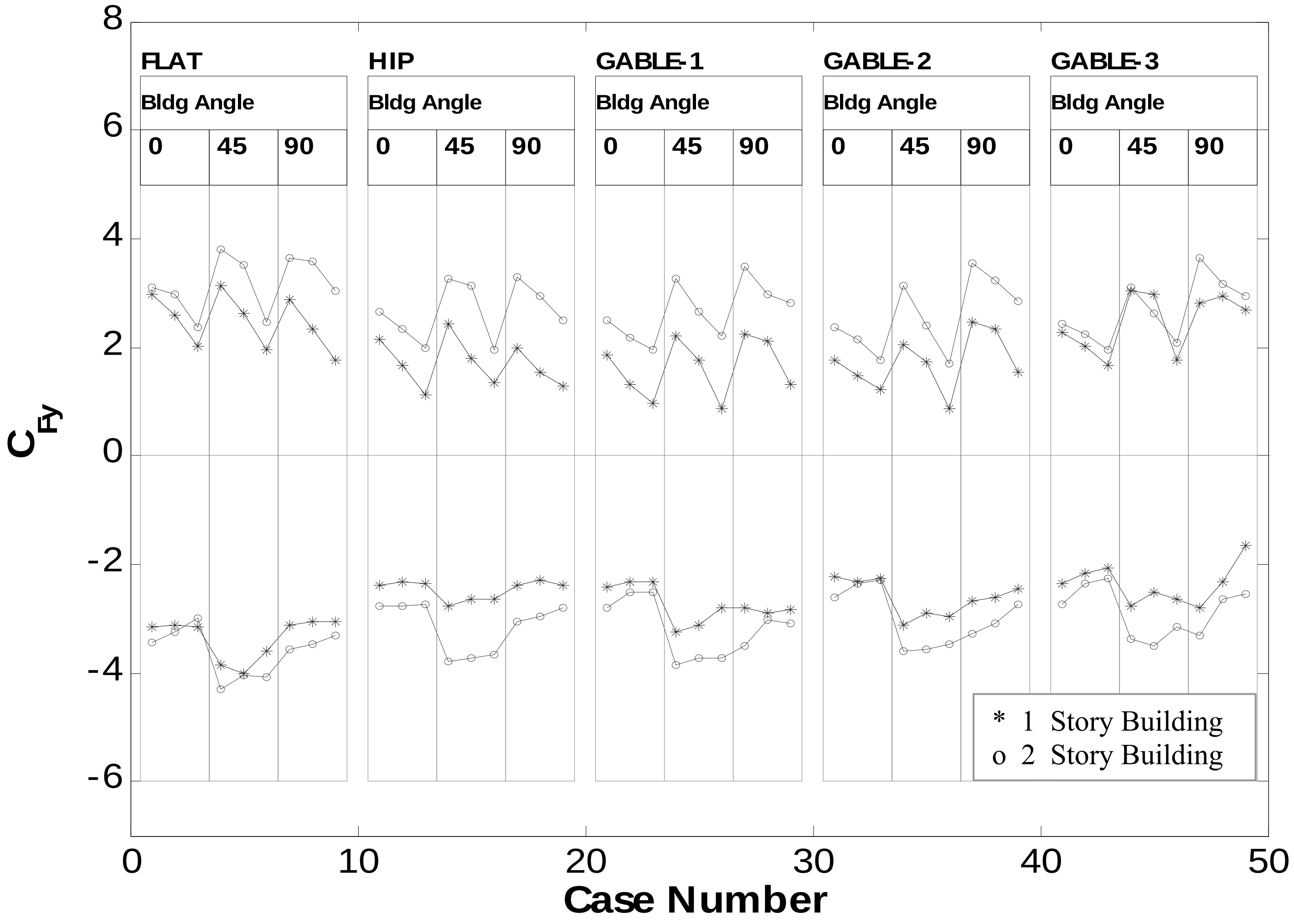

Figure 3-12: Maximum and minimum C_{Fy} for different building models

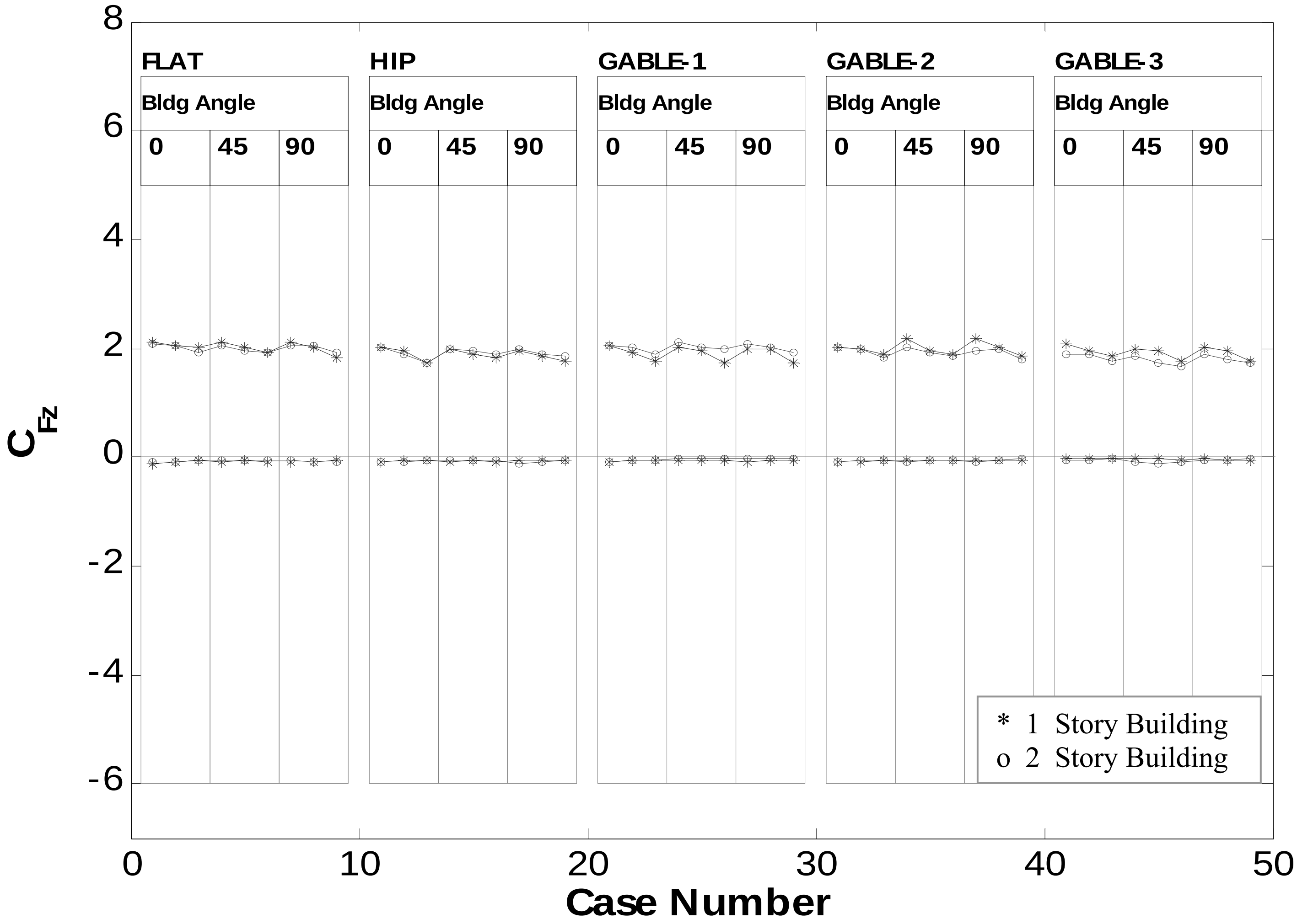

Figure 3-13: Maximum and minimum C_{Fz} for different building models

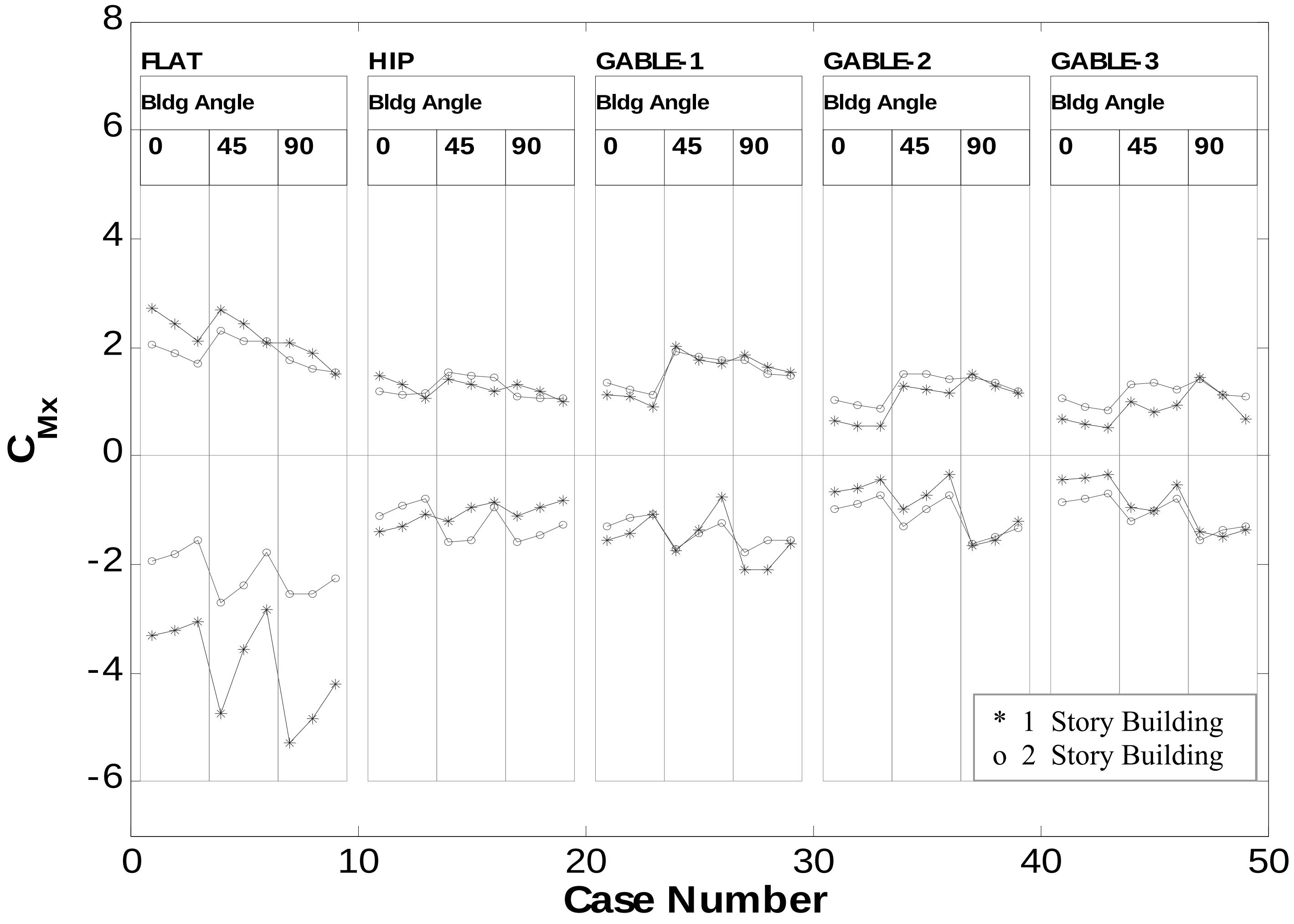

Figure 3-14: Maximum and minimum C_{Mx} for different building models

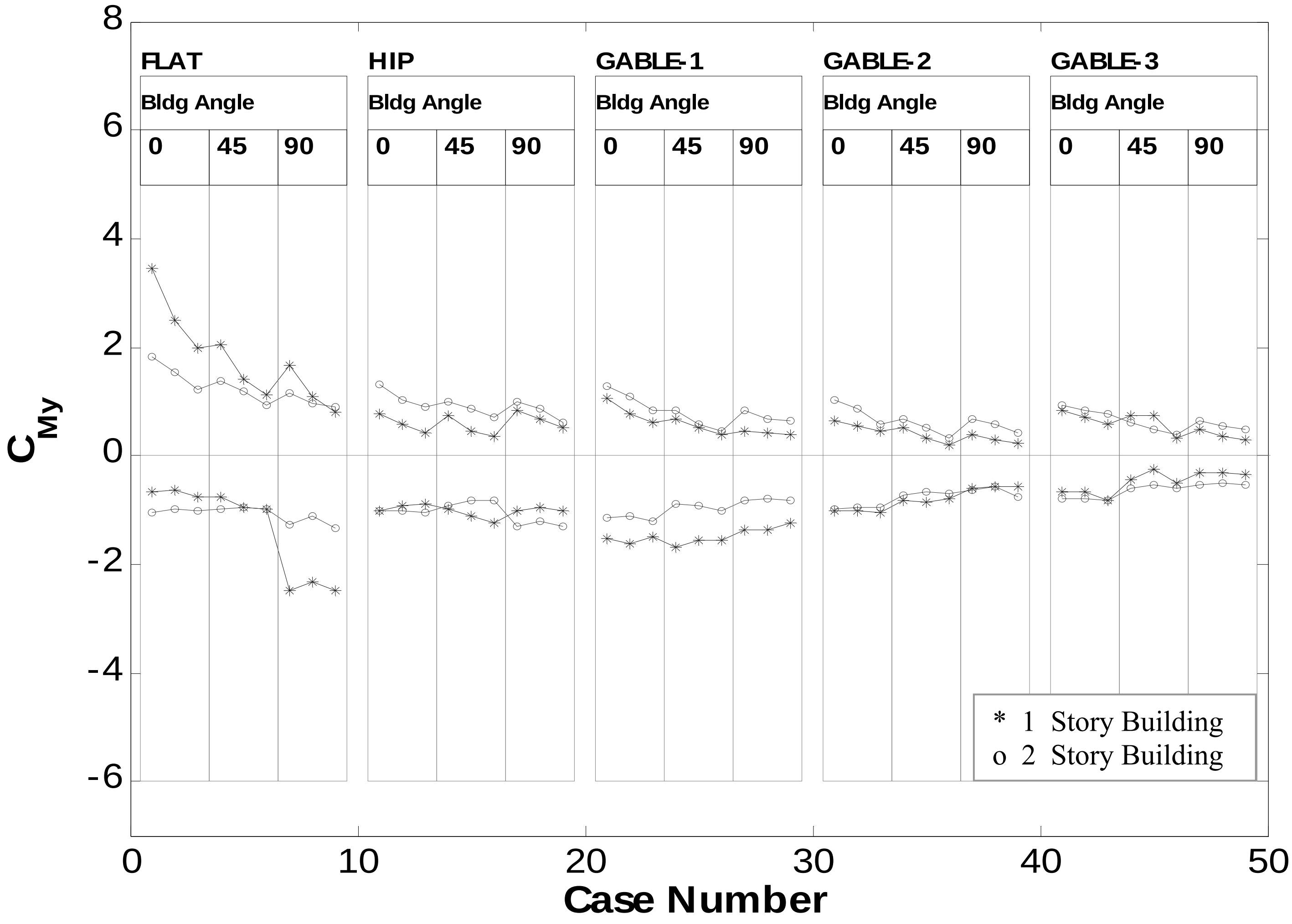

Figure 3-15: Maximum and minimum C_{My} for different building models

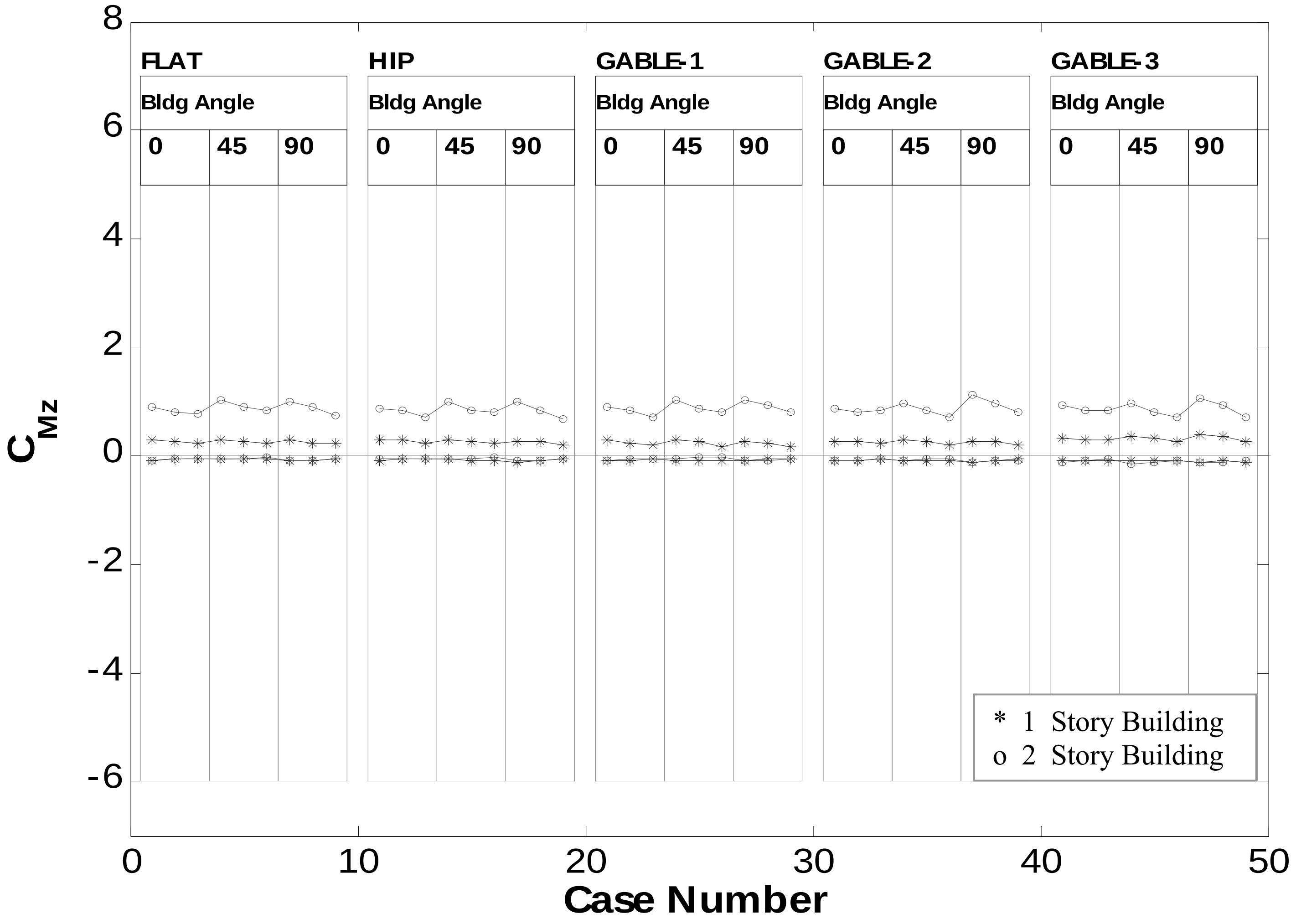

Figure 3-16: Maximum and minimum C_{Mz} for different building models

Model No.	Building Type	h/L *Full scale*	L/B *Full scale*	Angle of the Roof, Type	Terrain	Model Scale and Exp Type
1	Residential 1-Story	0.36 $h = 3.29$ m $h_E = 3.29$ m	1 $L = 9.2$ m $B = 9.2$ m	$\theta = 0^{o}$, Flat Roof	Smooth Open	1:100 Pressure
2	Residential 1-Story	0.454 $h = 4.18$ m $h_E = 2.99$ m	1 $L = 9.2$ m $B = 9.2$ m	$\theta = 14.5^{o}$, Hip Roof	Smooth Open	1:100 Pressure
3	Residential 1-Story	0.479 $h = 4.42$ m $h_E = 3.32$ m	1 $L = 9.2$ m $B = 9.2$ m	$\theta = 13.4^{o}$, Gable Roof	Smooth Open	1:100 Pressure
4	Residential 1-Story	0.599 $h = 5.52$ m $h_E = 3.32$ m	1 $L = 9.2$ m $B = 9.2$ m	$\theta = 25.5^{o}$, Gable Roof	Smooth Open	1:100 Pressure
5	Residential 1-Story	0.725 $h = 6.66$ m $h_E = 3.44$ m	1 $L = 9.2$ m $B = 9.2$ m	$\theta = 35.1^{o}$, Gable Roof	Smooth Open	1:100 Pressure
6	Residential 2-Story	0.699 $h = 6.43$ m $h_E = 6.43$ m	1 $L = 9.2$ m $B = 9.2$ m	$\theta = 0^{o}$, Flat Roof	Smooth Open	1:100 Pressure
7	Residential 2-Story	0.795 $h = 7.35$ m $h_E = 6.16$ m	1 $L = 9.2$ m $B = 9.2$ m	$\theta = 14.5^{o}$, Hip Roof	Smooth Open	1:100 Pressure
8	Residential 2-Story	0.821 $h = 7.56$ m $h_E = 6.48$ m	1 $L = 9.2$ m $B = 9.2$ m	$\theta = 13.4^{o}$, Gable Roof	Smooth Open	1:100 Pressure
9	Residential 2-Story	0.940 $h = 8.66$ m $h_E = 6.48$ m	1 $L = 9.2$ m $B = 9.2$ m	$\theta = 25.5^{o}$, Gable Roof	Smooth Open	1:100 Pressure
10	Residential 2-Story	1.07 $h = 9.81$ m $h_E = 6.58$ m	1 $L = 9.2$ m $B = 9.2$ m	$\theta = 35.1^{o}$, Gable Roof	Smooth Open	1:100 Pressure

Models are scaled on the basis of the above full-scale dimensions and the specified model scale. Model dimensions are scaled dimensions ± 0.25 mm.

L = Length, B = Width, h_E = Height at Eave, h = Total Height, θ = Roof Angle

Table 3-1: Description of the different building model tested

Bldg. Angle	Flat			Hip			Gable-1			Gable-2			Gable-3		
	TS1	TS2	TS3	TS1	TS2	TS3	TS1	TS2	TS3	TS1	TS2	TS3	TS1	TS2	TS3
0	1	2	3	10	11	12	19	20	21	28	29	30	37	38	39
45	4	5	6	13	14	15	22	23	24	31	32	33	40	41	42
90	7	8	9	16	17	18	25	26	27	34	35	36	43	44	45

Table 3-2: Description of the Test Matrix. All test cases are for Pressure measurement.

CHAPTER 4. CONCLUSION AND FUTURE WORK

4.1 Conclusion

The following conclusions are made for the 1:100 scale one story gable roof building with a roof angle of 35^0. In general,

- The slower translation speed results in greater loads on the building
- Tornado with smaller core radius generates more loads in the *x-y* plane
- The peak values of side force coefficients exceed by a factor of 2.09
- The peak values of uplift force coefficients exceed by a factor of 3.7
- Buildings constructed based of standard building codes will not withstand the wind loads created by tornadoes of F2 intensity.

The results from the different building model cases are summarized below,

- The flat roof and gable roof s show the effect of height in the C_{F_x} component
- The Side force C_{F_y} shows appreciable change irrespective of the roof types.
- The uplift force C_{F_z} does not change with roof types or height variations.
- The C_{M_x} and C_{M_y} coefficients variation is higher for flat roof, followed by gable and hip roof.
- The twisting moment is consistently higher for the 2 story case.

4.2 Future work

The current research tried to understand the effects of tornado winds on particular types of low-rise buildings. Few recommendations for future work.

- Effect of terrain – the present work is carried out for a smooth terrain. Different terrains can be simulated using various surface roughness and their effects on the structure of the vortex and the interaction with the building models can be studied.
- Effect of surrounding – currently the building model is tested in an isolated setup, hence by creating a urban/sub-urban landscape, the effects of surrounding can be studied in detail
- PIV based testing can be adopted to study the flow pattern over the building model. The same can be used to understand the vortex structure.
- Hot wire measurements can be done to find the effects of averaging time
- The internal pressure measurements should be carried out to estimate the actual uplift force.

APPENDIX: ADDITIONAL MATERIAL

Background

This section gives additional information regarding the vortex structure generated in the ISU Tornado simulator. The following passages are an excerpt from *"Design, Construction and Performance of a Large Tornado Simulator for Wind Engineering Applications - Engineering Structures in press, Dr Haan et al, 2007"*. The sections related to the radial and azimuthal velocity profiles of the vortex corresponding to different vane angles are discussed here.

Abstract

A laboratory tornado simulator was designed, constructed and tested to generate tornado like vortices for the purpose of quantifying tornado-induced aerodynamic loads on civil engineering structures. This simulator generates a vortex that can translate along a ground plane to interact with models of structures on the ground. The simulator uses a "rotating forced downdraft" technique that loosely matches the rear flank downdraft (RFD) phenomenon often emphasized as important to tornado genesis. The rotating forced downdraft is generated using a 1.83m diameter fan and two circular, sheet metal ducts suspended from an overhead crane that can translate along a 10.4m ground plane. Measurements were conducted to quantify the simulator's flow structures. An 18-hole pressure probe was used to traverse and map the vortex flow field. The flow structures of the

vortices were validated by comparing with mobile Doppler radar observations of two major tornados. Results show that tornado vortex radii from 0.23m to 0.56m can be generated. A wide range of maximum azimuthal velocities are also possible (from 6.9 m/s to 14.5 m/s). The simulator generates a range of vortex structures from single-celled vortices to two-celled vortices with corresponding swirl ratios ranging from 0.08 to 1.14. Comparisons of general flow structure and normalized profiles of azimuthal velocity showed excellent match between simulator and radar data. The range of tornado sizes together with model structures of 1/100 to 1/500 scales will allow extensive examination of tornado-induced wind loads on terrestrial structures. The effects of a tornado's size, translation speed and detailed flow structure on these loads can now be studied.

Vortex Structure

To illustrate the correlation between swirl ratio and the tornado core structure, Figure 2 shows velocity fields measured for laboratory vortices of low and high swirl ratio (S values of 0.08 and 1.14 for cases Vane1 and Vane5, respectively). In the case of the low swirl ratio, the flow in the *rz*-plane shows air moving downward from the outer downdraft duct, radially inward toward the vortex and then upward along the axis of the vortex. As the swirl ratio increases (with an accompanying decrease in flow rate into the vortex), the flow structure shows evidence of the evolution from a one-celled vortex to a drowned vortex jump (DVJ). That is, one observes a downward axial flow in the center of the vortex that does not reach the ground. Further increases in swirl ratio should show the vortex progress to a two-celled vortex as the axial flow reaches the ground plane. These observations are consistent with the trends observed by Church et al. [6]. These flow structure trends are also reflected in the surface pressure coefficient profiles shown in Figure 3. The flattened profile is due to the central downdraft along the vortex axis (also observed by Bienkiewicz and Dudhia [2]).

Figure 4 shows contour plots of azimuthal velocity for both the Spencer and Mulhall tornados. The flow structure is very similar to that of the laboratory vortex. The radius of maximum winds (RMW) will, in this paper, also be referred to as the radius of the core, c r .It is smallest directly adjacent to the surface and increases to a constant value quite close to the ground (typically less than 0.25 r_c). Even though these two tornados had significantly different sizes (RMW's were approximately 250-400m and 800m for Spencer and Mulhall tornados, respectively), their overall structures scale with each other quite well. This scaling can be seen more clearly when scaled azimuthal velocity profiles are plotted as in Figure 5. These profiles show how similar the laboratory and full scale tornado vortices are to each other. The bump in the radar profiles for r/r_c values greater than 2 is likely a result of the axisymmetric assumption (used in the radar data reduction approach) breaking down with distance from the core (Wurman [33]). Azimuthal velocity profiles are discussed further in the next section. Note (from Figure 4) that the wind speeds at the lowest elevation (20 m) were the strongest anywhere within the lowest kilometer. In addition, the radius of maximum winds is smaller at the lowest two heights and then becomes wider and relatively constant with height above roughly 70 m.

Azimuthal Velocity Profiles

Normalized azimuthal velocity profiles at various elevations are shown in Figure 6. Scaling the vortices with the core radius, r_c, and with the maximum azimuthal velocity, $V_{\theta max}$, collapses the data very well. The scaling tends to break down some what with distance from the center of the core. The scaling applies equally well to vortices over a wide range of swirl ratios as shown in Figure 7. With swirl ratios varying from 0.08 to 1.14, this profile is consistent. It is important that this facility have the capability to control the diameter of the vortex. To test the effect of the size of the vortex relative to the size of the building/structural model, one must be able to vary the vortex diameter. The most obvious way to control the diameter would be to control the swirl ratio. The most direct control of the swirl ratio in this facility comes from changing the angles of the vanes at the top of the simulator (see Figure 1). Increasing the vane angle increases the amount of circulation entering the vortex flow field and therefore increases the swirl ratio. It would be nice if this increase in circulation were not accompanied by a decrease in total flow rate through the system (the denominator of the swirl ratio), but these two quantities cannot be controlled separately in this system. Figure 8 shows azimuthal profiles for a wide range of vane angles (15° to 55°) with other simulator controls held constant. To illustrate the simulator's control of the size of the vortex, these profiles are normalized with the maximum velocity and the radius of the case Vane3. The size of the vortex varies by a factor of 2.3 from the smallest to the largest. These sizes correspond to vortex diameters from 0.23m to0.53m.

Radial Velocity Profiles

Radial velocity profiles at various distances from the center of the vortex were also plotted for a large and a small swirl ratio (the Vane1 and Vane5 cases). Figure 9 shows radial profiles for the Vane1 and the Vane5 cases to illustrate the dependence on swirl ratio. Figure 10 contains these same type of radial velocity profiles for the Doppler radar data from the Spencer and Mulhall tornados (Wurman [33, 34]). In both lab and full-scale cases, the radial flow tends to be strongest relatively far from the center of the vortex. Two observations can be made from a comparison between the simulator and radar data. First, the simulator's radial velocities are a much greater fraction of the maximum azimuthal velocity than is reflected in the radar data. And second, the radar data shows an increase in velocity for lower elevations that is only slightly evident in the simulator data. The radial inflow is strongest at the lowest elevation for all radial distances observed. This is also consistent with anecdotal evidence from storm chasers that describe very high velocities very close to the ground. These observations suggest the need for further work with the surface roughness of the simulator ground plane to improve this aspect of the full scale comparison.

Conclusion

A measurement campaign was conducted to quantify vortex flow structures and vortex dimensions that could be induced with the tornado simulator. Average three dimensional velocity components were obtained by sweeping an 18-hole pressure probe through a large region of the vortex flow field. Measurements of flow structure were validated by comparing with mobile Doppler radar observations of two major tornados.

Tornado vortex radii from 0.23m to 0.56m were generated with maximum azimuthal velocities ranging from 6.9 m/s to 14.5 m/s. When scaled with the radius of maximum azimuthal wind speed and the maximum azimuthal speed, velocity profiles collapsed very well—both lab data and radar data from the field. Single-celled vortices and two-celled vortices were generated with corresponding swirl ratios ranging from 0.08to 1.14. The range of tornado sizes and structures will allow extensive examination of tornado-induced wind loads on buildings and other structures. Using this facility, the effects of tornado size and tornado flow structure on aerodynamic loading can now be studied.

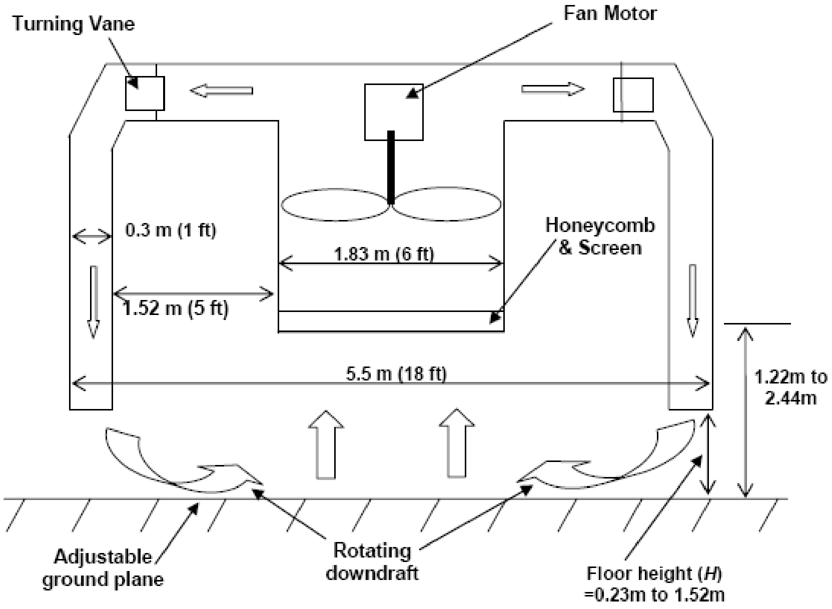

Figure 1: Schematic illustration of the tornado simulator.

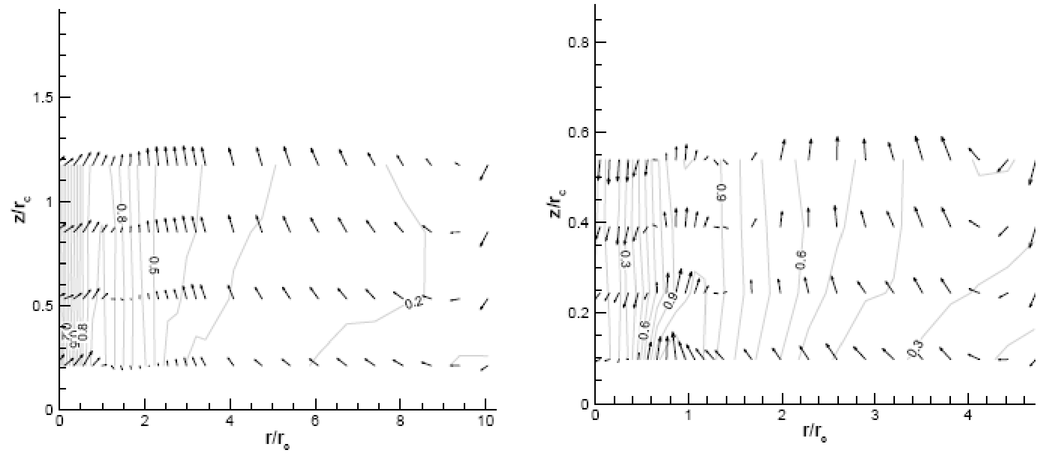

Figure 2: Contour and vector plots to show tornado corner flow structure. The contour labels denote azimuthal velocity (normalized lized with $V_{\theta \max}$) while the vectors show radial and vertical velocity. The small swirl ratio, *S*, for (a) is 0.08 (case Vane1), and the high swirl ratio for (b) is 1.14 (case Vane5). The large swirl ratio case exhibits the structure of a drowned vortex jump well on its way to a two-celled structure.

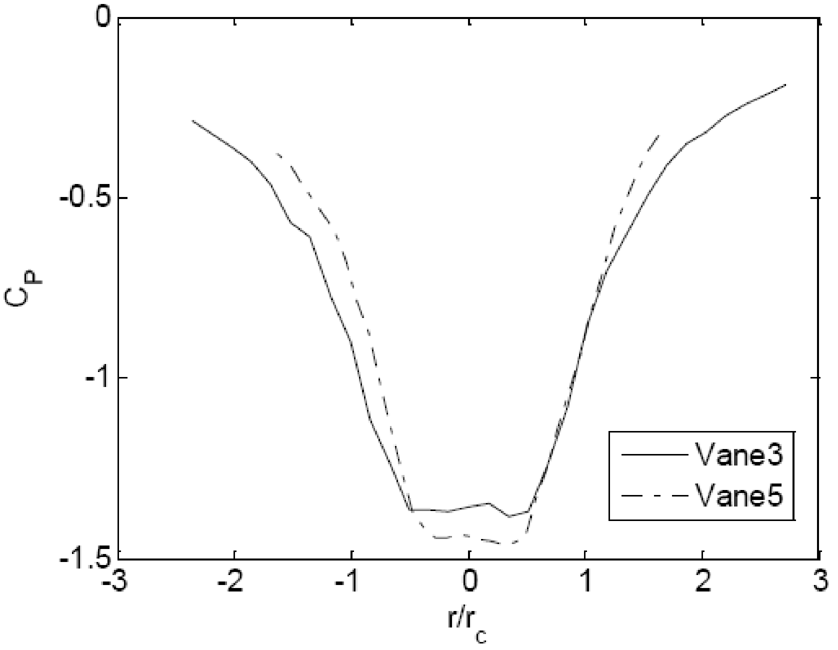

Figure 3: Surface pressure coefficient profiles for Vane3 and Vane5 cases. The pressure coefficient is calculated with static pressure outside the simulator as the reference pressure and $V_{\theta\,\max}$ to calculate dynamic pressure.

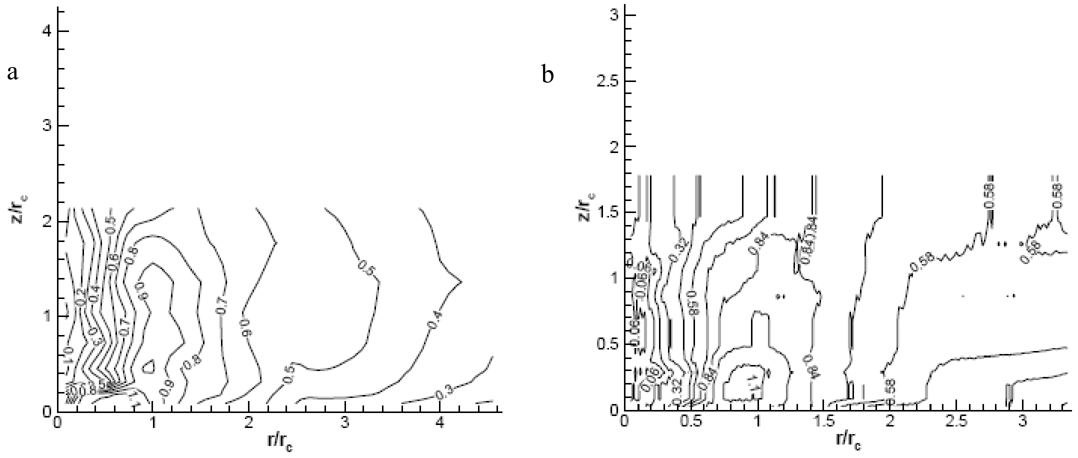

Figure 4: Contour plots of azimuthal velocity magnitudes (normalized lized with $V_{\theta\,\max}$) for (a) Spencer and (b) Mulhall tornados (Spencer and Mulhall core radii were approximately 225m and 900-1000m, respectively). The overall structure matches well with laboratory simulations.

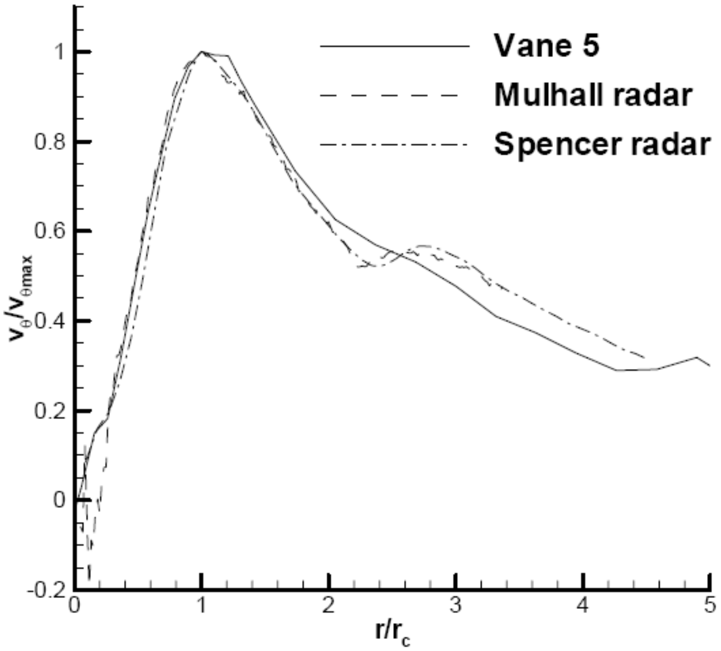

Figure 5: Scaled azimuthal velocity profiles for laboratory tornado case Vane5 and the Mulhall and Spencer tornado radar data. In each case, the elevation of the velocity profile was $z = 0.5r_c$ where r_c is the radius of maximum azimuthal wind speed.

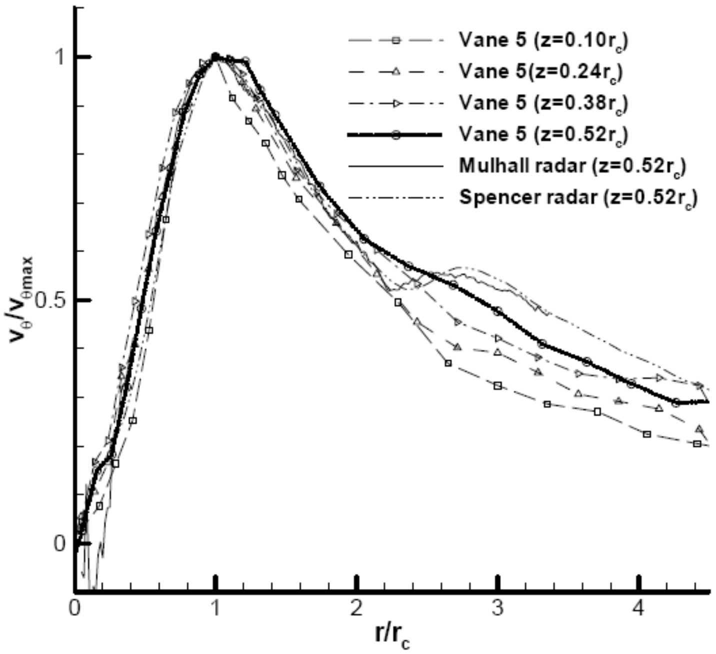

Figure 6: Scaled azimuthal velocity profiles for laboratory tornado case Vane5 at different elevations along with Mulhall and Spencer data at a specific elevation.

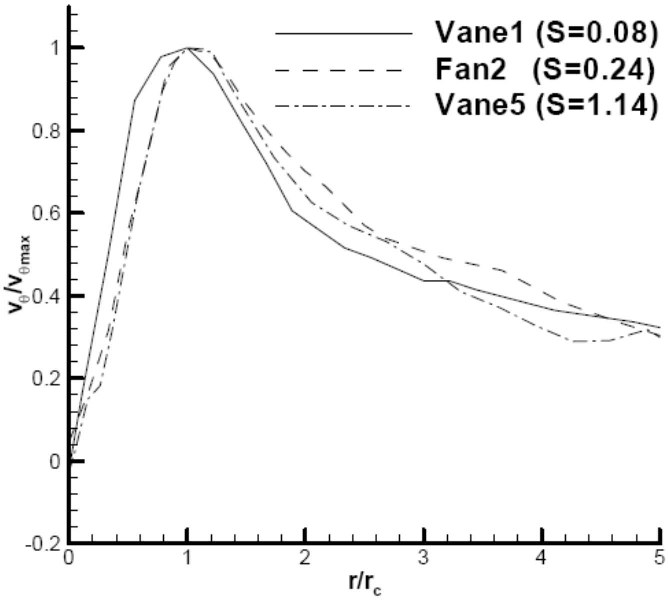

Figure 7: Normalized azimuthal velocity profiles showing collapse of data for a range of swirl ratios, *S* .

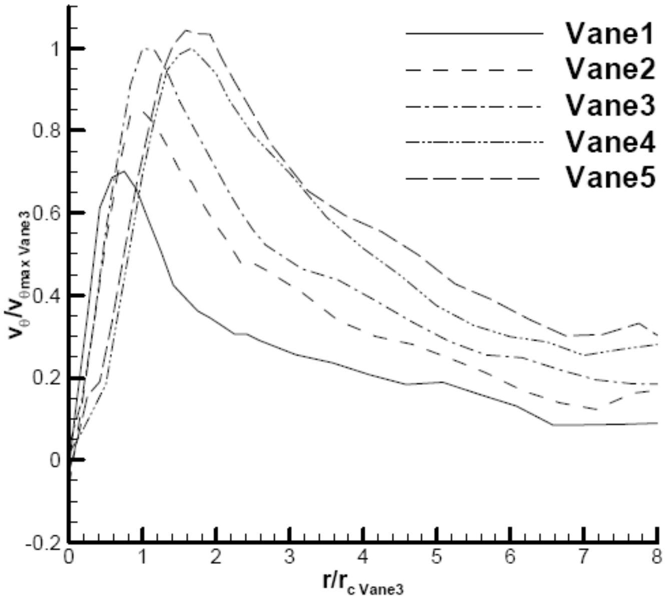

Figure 8: Azimuthal profiles showing the change of vortex core radius with increasing vane angle. Core radius can be increased by a factor of 2.3 by changing the vane angle.

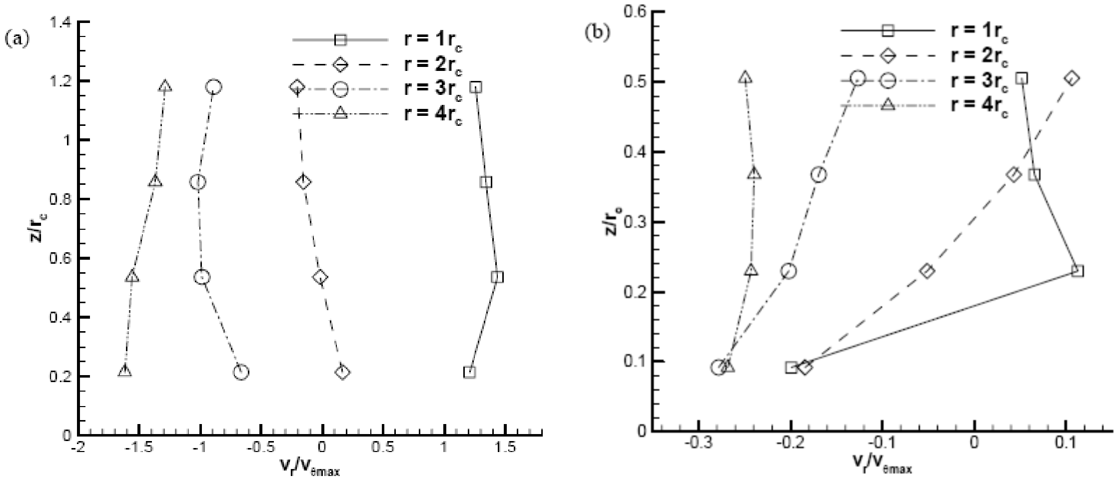

Figure 9: Normalized radial velocity profiles for (a) the Vane1 case (the smallest swirl ratio case) and (b) the Vane 5 case (the largest swirl ratio case) at various distances, *r*, from the center of the vortex.

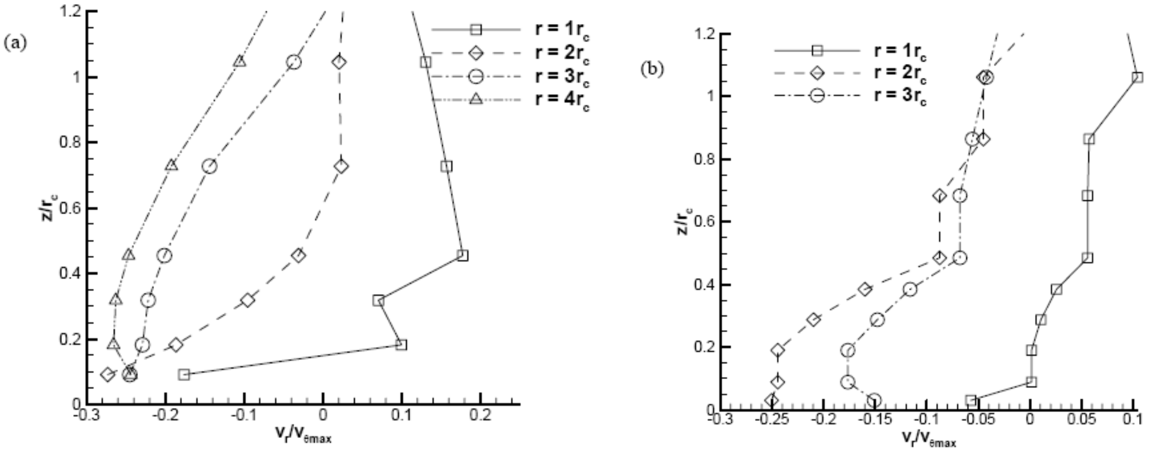

Figure 10: Normalized radial velocity profiles from Doppler radar data for the (a) Spencer tornado and the (b) Mulhall tornado at various distances, r, from the center of the vortex. These data are from Wurman (2004, 2005).

REFERENCES

[1] Alexander, C.R., Wurman, J., “The 30 May 1998 Spencer, South Dakota, storm. Part I: The structural evolution and environment of the tornadoes,” AMS Monthly Weather Review, v. 133, (2005) 72-96.

[2] Bienkiewicz, B., Dudhia, P. “Physical Modeling of Tornado-Like Flow and Tornado Effects on Building Loading,” Proc. Seventh U.S. National Conference on Wind Engineering (1993) 95-106.

[3] Bluestein, H.B., Golden, J., “A review of tornado observations,” in Church, Burgess, Doswell, Davies-Jones, Eds., The tornado: Its structure, dynamics, prediction, and hazards, American Geo. Mon., v. 79 (1993).

[4] Bluestein, B. H., Pazmany, L.A., “Observations of tornadoes and other convective phenomena with a mobile 3-mm wavelength Doppler radar: The spring 1999 field experiment,” Bulletin of the American Meteorological Society, v. 81 (2000) 2939-2951.

[5] Chang, C.C., “Tornado effects on buildings and structures with laboratory simulation,” Proc. Third International Conference on Wind Effects on Buildings and Structures, Tokyo, Japan (1971) 231-240.

[6] Church, C.R., Snow, J. T., Baker, G. L., Agee, E. M., “Characteristics of tornado-like vortices as a function of swirl ratio: A laboratory investigation,” Journal of the Atmospheric Sciences, v. 36 (1979) 1755-1776.

[7] Church, C. R., J. T. Snow, and E. M. Agee, “Tornado vortex simulation at Purdue University,” Bulletin of the American Meteorological Society, v. 58 (1977) 900-908.

[8] Davies-Jones, R.P. "Laboratory Simulation of Tornadoes," Proceedings of the Symposium on Tornadoes, Assessment of Knowledge and Implications for Man, Ed. R.E. Peterson, Texas Tech University (1976) 151-174.

[9] Davies-Jones, R.P., "The dependence of core radius on swirl ratio in a tornado simulator," Journal of the Atmospheric Sciences, v. 30 (1973) 1427-1430.

[10] Diamond C. J., and E. M. Wilkins, "Translation effects on simulated tornadoes," Journal of the Atmospheric Sciences, v. 41 (1984) 2574-2580.

[11] Fiedler, B.H., "Numerical simulation of axisymmetric tornadogenesis in forced convection," in C. Church et al., eds., The Tornado: its structure, dynamics, prediction and hazards, American Geophysical Union, Washington, D.C. (1993).

[12] Fiedler, B.H., "The thermodynamic speed limit and its violation in axisymmetric numerical simulations of tornado-like vortices," Atmosphere-Ocean, v. 32 (1994) 335-359.20

[13] Howells, P.C., Rotunno, R., Smith, R.K., "A comparative study of atmospheric and laboratory analogue numerical tornado-vortex models," Q.J. Royal Meteorological Society, v. 114 (1988) 801-822.

[14] Jischke, M. C., Light, B. D., "Laboratory simulation of tornadic wind loads on a rectangular model structure," Proc. Sixth International Conference on Wind Engineering, Australia & New Zealand, v. 1 (1983).

[15] Kardell, R.D., "Design and Testing of a Laboratory Tornado Simulator for the Purpose of Wind Engineering," M.S. Thesis, Iowa State University (2004).

[16] Lee, W.C., Wurman, J., “Diagnosed structure of the Mulhall tornado using VTD algorithm,” Preprints, 21st Conf. on Severe Local Storms, American Meteorological Society, San Antonio, TX, (2002) 217-220.

[17] Leslie, F. W., “Surface roughness effects on suction vortex formation,” Journal of the Atmospheric Sciences, v. 34 (1977) 1022-1027.

[18] Lewellen, W. S., “Tornado Vortex Theory,” in Church et al., eds., The Tornado: Its Structure, Dynamics, Prediction, and Hazards, Geophysical Monograph 79, American Geophysical Union, (1993) 19-39.

[19] Lewellen, D.C., Lewellen, W.S., “Large-Eddy Simulation of a Tornado’s Interaction with the Surface,” Journal of the Atmospheric Sciences, v. 54, n. 5 (1997) 581-605.

[20] Lewellen, W. S, Lewellen, D. C., Xia, J., “The influence of a local swirl ratio on tornado intensification near the surface,” Journal of the Atmospheric Sciences, v. 57 (1999) 527-544.

[21] Markowski, P. M., “Hook echoes and rear-flank downdrafts: A review”, Monthly Weather Review, v. 130 (2002) 852-876.

[22] Nolan, D.S., “A New Scaling for Tornado-Like Vortices,” Journal of the Atmospheric Sciences, v. 62 (2005) 2639-2645.

[23] Nolan, D.S., Farrell, B.F., “The structure and dynamics of tornado-like vortices,” Journal of the Atmospheric Sciences, v. 56 (1999) 2908-2936.

[24] Nolan, D.S., Almgren, A.S., Bell, J.B., “Studies of the relationship between the structure and dynamics of tornado-like vortices and their environmental forcing,” Lawrence Berkeley National Laboratory Report LBNL-47554 (2000).

[25] Rasmussen, E.N., Straka, J.M., Davies-Jones, R., Dowell III, C.A., Carr, F.H., Eilts, M. D., MacGorman, D.R., “Verification of the origins of rotation in tornadoes experiment: VORTEX,” Bulletin of the American Meteorological Society, v. 75 (1994) 995-1006.21

[26] Rotunno, R., “A Study in Tornado-like Vortex Dynamics,” Journal of the Atmospheric Sciences, v. 36 (1979) 140-155.

[27] Samaras, T., Lee, J.J., “Measuring Tornado Dynamics with In-Situ Instrumentation,” Proceedings, ASCE Structures Congress (2006).

[28] Wakimoto, R. M., Wilson, J. W., “Non-supercell tornadoes,” Monthly Weather Review, v. 117 (1989) 1113-1140.

[29] Ward, N.B., “The exploration of certain features of tornado dynamics using a laboratory model,” Journal of the Atmospheric Sciences, v. 29 (1972) 1194-1204.

[30] Wind Hazard Reduction Coalition, Date Accessed: Jan. 31, 2006
<http://www.windhazards.org>

[31] Wurman, J., Gill, S., Fine scale radar observations of the Dimmitt, Texas (2 June 1995), tornado, AMS Monthly Weather Review, v. 128, (2000) 2135-2164.

[32] Wurman, J., Alexander, C.R., “The 30 May 1998 Spencer, South Dakota, storm. Part II: Comparison of observed damage and radar-derived winds in the tornadoes,” AMS Monthly Weather Review, v. 133, (2005) 97-118.

[33] Wurman, J., Personal Communication (2004).

[34] Wurman, J., Personal Communication (2005).